## NEW OPTIMIZED ROBIN–ROBIN DOMAIN DECOMPOSITION METHODS USING KRYLOV SOLVERS FOR THE STOKES–DARCY SYSTEM\*

YINGZHI LIU<sup>†</sup>, YASSINE BOUBENDIR<sup>‡</sup>, XIAOMING HE<sup>§</sup>, AND YINNIAN HE<sup>¶</sup>

**Abstract.** In this paper, we are interested in the design of optimized Schwarz domain decomposition algorithms to accelerate the Krylov type solution for the Stokes–Darcy system. We use particular solutions of this system on a circular geometry to analyze the iteration operator mode by mode. We introduce a new optimization strategy of the so-called Robin parameters based on a specific linear relation between these parameters, using the min-max and the expectation minimization approaches. Moreover, we use a Krylov solver to deal with the iteration operator and accelerate this new optimized domain decomposition algorithm. Several numerical experiments are provided to validate the effectiveness of this new method.

**Key words.** Stokes–Darcy system, domain decomposition methods, Robin interface conditions, modal analysis, optimized Schwarz methods, Krylov solvers

MSC codes. 65N55, 65F10

**DOI.** 10.1137/21M1417223

1. Introduction. The Stokes–Darcy model, which couples the fluid flow and porous media flow, arises in many applications, such as interaction between surface and subsurface flows [13, 16, 47], petroleum extraction [1, 31, 32, 41, 42, 54], and industrial filtration [24]. The Stokes and Darcy flows are coupled through three interface conditions including the one describing the conservation of mass, the condition describing the balance of the forces, and the Beavers–Joseph–Saffman–Jones (BJSJ) [45, 59] interface condition. Due to the numerical complexity of this coupled system, several methods have been developed to efficiently solve this problem including domain decomposition algorithms [7, 10, 18, 19, 21, 22, 37, 39, 40, 52, 60], Lagrange multiplier and partitioned time stepping methods [20, 33, 48, 56], discontinuous Galerkin and coupled finite element methods [3, 11, 8, 15, 36, 43, 46, 51, 57], and many others [2, 6, 38, 49, 55, 61]. Because Stokes and Darcy equations are coupled through a common interface using suitable conditions, it is appropriate to use nonoverlapping domain decomposition methods to reduce the original coupled system to two separate problems solved independently by using adequate methods in each subdomain.

It is well known that the Robin type domain decomposition method (DDM) is an effective technique for second-order elliptic problems originally introduced by Lions

<sup>\*</sup>Submitted to the journal's Computational Methods in Science and Engineering section May 3, 2021; accepted for publication (in revised form) April 14, 2022; published electronically August 22, 2022.

 $<sup>\</sup>rm https://doi.org/10.1137/21M1417223$ 

**Funding:** The work of the second author was supported by the NSF through grants DMS-1720014 and DMS-2011843. The work of the third author was supported by the NSF through grant DMS-1722647.

<sup>&</sup>lt;sup>†</sup>Department of Mathematics, University of Macau, Macau, People's Republic of China (yingzhiliu@um.edu.mo).

<sup>&</sup>lt;sup>‡</sup>Department of Mathematical Sciences and Center for Applied Mathematics and Statistics, New Jersey Institute of Technology, University Heights, Newark, NJ 07102 USA (boubendi@njit.edu).

<sup>§</sup>Department of Mathematics and Statistics, Missouri University of Science and Technology, Rolla, MO 65409 USA (hex@mst.edu).

<sup>¶</sup>School of Mathematics and Statistics, Xi'an Jiaotong University, Xi'an, 710049, People's Republic of China (heyn@mail.xjtu.edu.cn).

in [50]. In the case here, the Robin transmission conditions with Robin parameters can be viewed as the zero-order approximation of optimal transmission conditions involving Dirichlet-to-Neumann operators [44]. Then the optimized Schwarz methods [25, 27, 30] further significantly enhanced DDM convergence properties. This resulted in many related research works mainly consisting of the design of robust DDM for various equations, such as the second-order elliptic equation [23, 26, 28, 53], the diffusion-reaction problems [4, 29, 34], the Stokes-Darcy model [17], the fluid-structure interaction with spherical interfaces [35], and many others.

The aim of this work consists of improving the Robin–Robin DDM algorithm proposed in [14] by optimizing the transmission conditions. Generally speaking, we propose to appropriately choose the Robin parameters by following the framework of the procedure performed in [17] where the authors used Fourier techniques to explicitly express the rate of convergence on a particular geometry with a straight line interface, and then derive these optimal parameters. The method in [17] led to a hyperbolic relation coupling these Robin parameters which, in turn, produced a robust and fast algorithm. In this paper, we follow a similar procedure on a circular geometry and propose a new relation between the Robin parameters. It is a linear equation based on the line which connects the two Robin parameter pairs for the minimum mode and the maximum mode of the hyperbolic relation.

To obtain the optimal Robin parameters in this paper in the case of the new proposed linear relation, we use the well-known min-max and expectation minimization techniques. For the min-max approach, we first prove that the maximum spectral radius using the corresponding optimal parameters to this relation is less than one. This result is also satisfied in the case of the hyperbolic relation introduced in [17]. In the context of some realistic values of hydraulic conductivity and viscosity, which are usually small in practice, we prove that the obtained maximum spectral radius using the linear relation is smaller than the one obtained with the hyperbolic relation. Indeed, Remark 5.11 provides several observations regarding the advantages of the linear relation. For the expectation approach, although the analysis is difficult due to the formula complexity, we observe an improved spectral distribution which will accelerate the convergence of the iterative method when using Krylov solvers [62, 58].

The rest of this paper is organized as follows. In section 2, we introduce the Stokes–Darcy system with the BJSJ interface condition. In section 3, we review the Robin–Robin DDM and the Robin transmission conditions. In section 4, we analyze the spectral radius of the iterative operator using a modal analysis. In section 5, we present and analyze the optimal Robin parameters corresponding to the new linear relation. In section 6, we describe the Krylov solver named Orthodir used in this work to deal with the iterative procedure. Finally, we provide some numerical experiments to confirm the effectiveness of the optimal Robin parameters in section 7 and draw the conclusion in section 8.

**2. Problem setting.** We consider the coupled Stokes–Darcy system on a bounded domain  $\Omega = \Omega_D \cup \Omega_S \subset \mathbb{R}^d$  (d = 2, 3), where  $\Omega_D$  is the porous media domain and  $\Omega_S$  is the free-flow domain; see Figure 1.

The free flow in  $\Omega_S$  can be governed by steady Stokes equations: find the fluid velocity  $\mathbf{u}_S$  and the kinematic pressure  $p_S$ , such that

$$(2.1) -\nabla \cdot \mathbb{T}(\boldsymbol{u}_S, p_S) = \boldsymbol{f}_S, \ \nabla \cdot \boldsymbol{u}_S = 0,$$

where  $\mathbb{T}(\boldsymbol{u}_S, p_S) = 2\mu \mathbb{D}(\boldsymbol{u}_S) - p_S \mathbb{I}$  is the stress tensor,  $\mathbb{D}(\boldsymbol{u}_S) = 1/2(\nabla \boldsymbol{u}_S + \nabla^T \boldsymbol{u}_S)$  is the deformation tensor,  $\mu$  is the kinematic viscosity of the fluid, and  $\boldsymbol{f}_S$  is a given

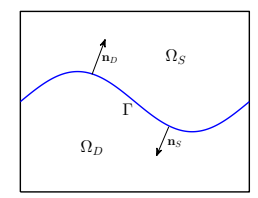


Fig. 1. Schematic of the computational domain with the interface  $\Gamma$ .

external force.

The porous media flow in  $\Omega_D$  can be described by Darcy equations: find the fluid velocity  $\mathbf{u}_D$  and the hydraulic head  $\phi_D$ , such that

$$(2.2) u_D = -\mathbb{K}\nabla\phi_D, \ \nabla\cdot\boldsymbol{u}_D = f_D,$$

where  $f_D$  is a source term and  $\mathbb{K}$  is the hydraulic conductivity tensor. In this paper, we assume that the media in  $\Omega_D$  is homogeneous isotropic, i.e.,  $\mathbb{K} = K\mathbb{I}$  with a constant K, and consider the following primary formulation for the Darcy system:

$$(2.3) -\nabla \cdot (\mathbb{K}\nabla \phi_D) = f_D.$$

Let  $\Gamma = \partial \Omega_D \cap \partial \Omega_S$  be the interface shared by the fluid and porous media regions. On the interface  $\Gamma$ , we consider the following three interface conditions: (2.4)

$$\boldsymbol{u}_S \cdot \boldsymbol{n}_S = -\boldsymbol{u}_D \cdot \boldsymbol{n}_D, \ -\boldsymbol{\tau}_j \cdot (\mathbb{T}(\boldsymbol{u}_S, p_S) \cdot \boldsymbol{n}_S) = \alpha \boldsymbol{\tau}_j \cdot \boldsymbol{u}_S, \ -\boldsymbol{n}_S \cdot (\mathbb{T}(\boldsymbol{u}_S, p_S) \cdot \boldsymbol{n}_S) = g(\phi_D - z),$$

where  $n_S$  and  $n_D$  denote the unit outer normal to the fluid and the porous media regions on the interface  $\Gamma$ , respectively,  $\tau_j$   $(j=1,\ldots,d-1)$  denote mutually orthogonal unit tangential vectors to the interface  $\Gamma$ ,  $\alpha$  is a constant depending on  $\mu$  and  $\mathbb{K}$ , gis the gravitational acceleration, and z is the height in the definition of the hydraulic head. The second condition is referred to as the BJSJ interface condition [45, 59].

We assume that the hydraulic head  $\phi_D$  and the fluid velocity  $\boldsymbol{u}_S$  satisfy the homogeneous Dirichlet boundary condition except on  $\Gamma$ , i.e.,  $\phi_D = 0$  on the boundary  $\partial \Omega_D \backslash \Gamma$  and  $\boldsymbol{u}_S = 0$  on the boundary  $\partial \Omega_S \backslash \Gamma$ .

The spaces that we utilize are

$$X_S = \{ \boldsymbol{v} \in [H^1(\Omega_S)]^d \mid \boldsymbol{v} = 0 \text{ on } \partial \Omega_S \backslash \Gamma \}, \quad Q_S = L^2(\Omega_S),$$
  
 $X_D = \{ \psi \in H^1(\Omega_D) \mid \psi = 0 \text{ on } \partial \Omega_D \backslash \Gamma \}.$ 

For the domain D ( $D = \Omega_S$  or  $\Omega_D$ ),  $(\cdot, \cdot)_D$  denotes the  $L^2$  inner product on the domain D, and  $\langle \cdot, \cdot \rangle$  denotes the  $L^2$  inner product on the interface  $\Gamma$  or the duality pairing between  $(H_{00}^{1/2}(\Gamma))'$  and  $H_{00}^{1/2}(\Gamma)$ .

With these notations, the weak formulation of the coupled Stokes–Darcy problem is given as follows [12, 22]: find  $(\boldsymbol{u}_S, p_S) \in X_S \times Q_S$  and  $\phi_D \in X_D$  such that

(2.5a)
$$a_{S}(\boldsymbol{u}_{S},\boldsymbol{v}) + b_{S}(\boldsymbol{v},p_{S}) + a_{D}(\phi_{D},\psi) + \langle g\phi_{D},\boldsymbol{v}\cdot\boldsymbol{n}_{S}\rangle - \langle \boldsymbol{u}_{S}\cdot\boldsymbol{n}_{S},\psi\rangle + \alpha\langle P_{\tau}(\boldsymbol{u}_{S}), P_{\tau}\boldsymbol{v}\rangle = (f_{D},\psi)_{\Omega_{D}} + (\boldsymbol{f}_{S},\boldsymbol{v})_{\Omega_{S}} + \langle gz,\boldsymbol{v}\cdot\boldsymbol{n}_{S}\rangle \quad \forall \ \boldsymbol{v}\in X_{S}, \ \psi\in X_{D},$$
(2.5b)
$$b_{S}(\boldsymbol{u}_{S},q) = 0 \qquad \forall \ q\in Q_{S},$$

where the bilinear forms are defined as

$$a_D(\phi_D, \psi) = (\mathbb{K}\nabla\phi_D, \nabla\psi)_{\Omega_D}, \ a_S(\boldsymbol{u}_S, \boldsymbol{v}) = 2\mu(\mathbb{D}(\boldsymbol{u}_S), \mathbb{D}(\boldsymbol{v}))_{\Omega_S},$$

$$(2.6) \qquad b_S(\boldsymbol{v}, q) = -(\nabla \cdot \boldsymbol{v}, q)_{\Omega_S},$$

and  $P_{\tau}$  denotes the projection onto the tangent space on  $\Gamma$ , i.e.,  $P_{\tau} \boldsymbol{u} = \sum_{j=1}^{d-1} (\boldsymbol{u} \cdot \boldsymbol{\tau}_j) \boldsymbol{\tau}_j$ . The system of (2.5a) and (2.5b) is well posed for  $\boldsymbol{f}_S \in [L^2(\Omega_S)]^d$ , as shown in [12, 22].

3. Nonoverlapping domain decomposition method. Let  $\gamma_f$  and  $\gamma_p$  be two positive constants called Robin parameters. For given functions  $\eta_f \in L^2(\Gamma)$  and  $\eta_p \in L^2(\Gamma)$ , we consider the Robin boundary conditions on the interface  $\Gamma$  for the Stokes and Darcy equations

(3.1) 
$$\boldsymbol{n}_S \cdot (\mathbb{T}(\boldsymbol{u}_S, p_S) \cdot \boldsymbol{n}_S) + \gamma_f \boldsymbol{u}_S \cdot \boldsymbol{n}_S = \eta_f, \quad \gamma_p \mathbb{K} \nabla \phi_D \cdot \boldsymbol{n}_D + g \phi_D = \eta_p.$$

Under these boundary conditions, the coupled weak formulation (2.5a)–(2.5b) can be decoupled as follows:

$$(3.2a) a_{S}(\boldsymbol{u}_{S}, \boldsymbol{v}) + b_{S}(\boldsymbol{v}, p_{S}) + \gamma_{f} \langle \boldsymbol{u}_{S} \cdot \boldsymbol{n}_{S}, \boldsymbol{v} \cdot \boldsymbol{n}_{S} \rangle + \alpha \langle P_{\tau} \boldsymbol{u}_{S}, P_{\tau} \boldsymbol{v} \rangle = (\boldsymbol{f}_{S}, \boldsymbol{v})_{\Omega_{S}} + \langle \eta_{f}, \boldsymbol{v} \cdot \boldsymbol{n}_{S} \rangle \quad \forall \, \boldsymbol{v} \in X_{S},$$

$$(3.2b) b_{S}(\boldsymbol{u}_{S}, q) = 0 \quad \forall \, q \in Q_{S},$$

and

(3.3) 
$$a_D(\phi_D, \psi) + \left\langle \frac{g\phi_D}{\gamma_p}, \psi \right\rangle = (f_D, \psi)_{\Omega_D} + \left\langle \frac{\eta_p}{\gamma_p}, \psi \right\rangle \qquad \forall \psi \in X_D.$$

The compatibility conditions for the equivalence between the coupled Stokes–Darcy system (2.5a)–(2.5b) and decoupled Stokes–Darcy system (3.2a)–(3.3) with Robin boundary conditions (3.1) at the interface  $\Gamma$  are given in [14] by

(3.4) 
$$\eta_f = \gamma_f \mathbf{u}_S \cdot \mathbf{n}_S - g\phi_D + gz, \quad \eta_p = \gamma_p \mathbf{u}_S \cdot \mathbf{n}_S + g\phi_D.$$

From (3.4), we have

(3.5a) 
$$\eta_{f} = \gamma_{f} \boldsymbol{u}_{S} \cdot \boldsymbol{n}_{S} - g\phi_{D} + gz = \gamma_{f} \left( \frac{1}{\gamma_{p}} (\eta_{p} - g\phi_{D}) \right) - g\phi_{D} + gz$$

$$= \frac{\gamma_{f}}{\gamma_{p}} \eta_{p} - \left( 1 + \frac{\gamma_{f}}{\gamma_{p}} \right) g\phi_{D} + gz,$$

$$\eta_{p} = \gamma_{p} \boldsymbol{u}_{S} \cdot \boldsymbol{n}_{S} + g\phi_{D} = \gamma_{p} \boldsymbol{u}_{S} \cdot \boldsymbol{n}_{S} + (-\eta_{f} + \gamma_{f} \boldsymbol{u}_{S} \cdot \boldsymbol{n}_{S} + gz)$$

$$= -\eta_{f} + (\gamma_{f} + \gamma_{p}) \boldsymbol{u}_{S} \cdot \boldsymbol{n}_{S} + gz.$$

Now we review the Robin–Robin domain decomposition algorithm [14]:

- 1. Give the initial values  $\eta_p^0$  and  $\eta_f^0$ .
- 2. For  $k=0,1,2,\ldots$ , independently solve the Stokes and Darcy systems with Robin boundary conditions. More precisely,  $\boldsymbol{u}_S^k \in X_S$  and  $p_S^k \in Q_S$  are computed from

(3.6a) 
$$a_{S}(\boldsymbol{u}_{S}^{k},\boldsymbol{v}) + b_{S}(\boldsymbol{v},p_{S}^{k}) + \gamma_{f}\langle\boldsymbol{u}_{S}^{k}\cdot\boldsymbol{n}_{S},\boldsymbol{v}\cdot\boldsymbol{n}_{S}\rangle + \alpha\langle P_{\tau}\boldsymbol{u}_{S}^{k},P_{\tau}\boldsymbol{v}\rangle$$
$$= \langle \eta_{f}^{k},\boldsymbol{v}\cdot\boldsymbol{n}_{S}\rangle + (\boldsymbol{f}_{S},\boldsymbol{v})_{\Omega_{S}} \quad \forall \boldsymbol{v} \in X_{S},$$
(3.6b) 
$$b_{S}(\boldsymbol{u}_{S}^{k},q) = 0 \quad \forall q \in Q_{S},$$

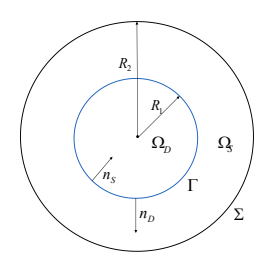


Fig. 2. A sketch of the circular domain.

and  $\phi_D^k \in X_D$  is computed from

$$(3.7) a_D(\phi_D^k, \psi) + \left\langle \frac{g\phi_D^k}{\gamma_p}, \psi \right\rangle = \left\langle \frac{\eta_p^k}{\gamma_p}, \psi \right\rangle + (f_D, \psi)_{\Omega_D} \forall \psi \in X_D.$$

3. Update  $\eta_p^{k+1}$  and  $\eta_f^{k+1}$ :

(3.8) 
$$\eta_f^{k+1} = a\eta_p^k + bg\phi_D^k + gz, \quad \eta_p^{k+1} = c\eta_f^k + d\mathbf{u}_S^k \cdot \mathbf{n}_S + gz,$$

where the coefficients a, b, c, d are chosen based on (3.5):

$$a = \frac{\gamma_f}{\gamma_p}, \quad b = -1 - a, \quad c = -1, \quad d = \gamma_f + \gamma_p.$$

**4. Modal analysis.** In order to optimize the convergence of the Robin–Robin algorithm by Krylov subspace method, we now use the modal analysis tool [5, 7, 27] to investigate convergence properties of the related iteration operator on a circular interface shown in Figure 2. For the sake of analysis, we assume that g = 1, z = 0.

Combining the Robin boundary conditions (3.1) with the updating processes (3.8) in the above Robin–Robin algorithm, we obtain (4.1)

$$\gamma_p \mathbb{K} \nabla \phi_D \cdot \boldsymbol{n}_D + \phi_D = c \eta_f + d\boldsymbol{u}_S \cdot \boldsymbol{n}_S, \quad \boldsymbol{n}_S \cdot (\mathbb{T}(\boldsymbol{u}_S, p_S) \cdot \boldsymbol{n}_S) + \gamma_f \boldsymbol{u}_S \cdot \boldsymbol{n}_S = a \eta_p + b \phi_D.$$

Our study is then reduced to the decoupled continuous Darcy problem

(4.2) 
$$\begin{cases} \boldsymbol{u}_D^k + \mathbb{K} \nabla \phi_D^k = 0, \ \nabla \cdot \boldsymbol{u}_D^k = 0 & \text{in } \Omega_D, \\ \gamma_p \mathbb{K} \nabla \phi_D^k \cdot \boldsymbol{n}_D + \phi_D^k = \eta_p^k & \text{on } \Gamma, \end{cases}$$

and the continuous Stokes problem

$$\begin{cases} \mu \Delta \boldsymbol{u}_{S}^{k} - \nabla p_{S}^{k} = 0, \ \nabla \cdot \boldsymbol{u}_{S}^{k} = 0 & \text{in } \Omega_{S}, \\ \boldsymbol{u}_{S}^{k} = 0 & \text{on } \Sigma, \\ \boldsymbol{u}_{S}^{k} \cdot \boldsymbol{\tau}_{S} = 0, \ \boldsymbol{n}_{S} \cdot (\mathbb{T}(\boldsymbol{u}_{S}^{k}, p_{S}^{k}) \cdot \boldsymbol{n}_{S}) + \gamma_{f} \boldsymbol{u}_{S}^{k} \cdot \boldsymbol{n}_{S} = \eta_{f}^{k} & \text{on } \Gamma, \end{cases}$$

where  $\Gamma = \partial \Omega_D \cap \partial \Omega_S$  and  $\Sigma = \partial \Omega_S \setminus \Gamma$ .

Performing one iteration with  $\eta^{k} = (\eta_f^k, \eta_p^k)^T$  consists of computing

(4.4) 
$$\eta^{k+1} = \begin{pmatrix} a\eta_p^k + b\phi_D^k \\ c\eta_f^k + d\boldsymbol{u}_S^k \cdot \boldsymbol{n}_S \end{pmatrix}.$$

From (4.4), we define the iteration operator of the algorithm  $\mathcal{A}: \eta \in (L^2(\Gamma))^2 \mapsto \mathcal{A}\eta \in (L^2(\Gamma))^2$  by

(4.5) 
$$\mathcal{A} = \begin{pmatrix} 0 & \mathcal{D} \\ \mathcal{S} & 0 \end{pmatrix},$$

where  $S: \eta_f \in L^2(\Gamma) \to S\eta_f \in L^2(\Gamma)$  is the Stokes component and  $\mathcal{D}: \eta_p \in L^2(\Gamma) \to \mathcal{D}\eta_p \in L^2(\Gamma)$  is the Darcy component. Following [7], we define the basis functions in  $L^2(\Gamma)$  by

$$H_m(\theta) = \frac{1}{\sqrt{2\pi}} e^{im\theta}, \quad \theta \in [0, 2\pi], \quad m \in \mathbf{Z},$$

then obtain the modal decomposition of the Darcy and Stokes operators.

PROPOSITION 4.1. The operator  $\mathcal{D}$  in (4.5), which is related to the Darcy problem (4.2) and defined from  $L^2(\Gamma)$  to  $L^2(\Gamma)$  by

$$\mathcal{D}\eta_p = a\eta_p + b\phi_D,$$

has the decomposition  $\mathcal{D}\eta_p = \sum_{m \in \mathbf{Z}} \mathcal{D}_m \eta_{p,m} H_m(\theta)$  with

(4.7) 
$$\mathcal{D}_0 = -1, \quad \mathcal{D}_m = \frac{\gamma_f K|m|/R_1 - 1}{\gamma_p K|m|/R_1 + 1} \quad (m \neq 0),$$

where  $\eta_p = \sum_{m \in \mathbb{Z}} \eta_{p,m} H_m(\theta)$ , and  $R_1$  is the radius of the Darcy domain  $\Omega_D$ .

*Proof.* Following the proof of Proposition 4.1 in [7] and using (4.2) and (4.6), we similarly obtain the modal coefficient  $\mathcal{D}_m$  in (4.7).

PROPOSITION 4.2. The operator S in (4.5), which is related to the Stokes problem (4.3) and defined from  $L^2(\Gamma)$  to  $L^2(\Gamma)$  by

$$\mathcal{S}\eta_f = c\eta_f + d\mathbf{u}_S \cdot \mathbf{n}_S,$$

has the decomposition  $S\eta_f = \sum_{m \in \mathbf{Z}} S_m \eta_{f,m} H_m(\theta)$  with

(4.9) 
$$S_0 = -1, \quad S_m = \frac{\gamma_p M_m / \mu - N_m}{\gamma_f M_m / \mu + N_m} \quad (m \neq 0).$$

where  $\eta_f = \sum_{m \in \mathbb{Z}} \eta_{f,m} H_m(\theta)$ , and  $M_m, N_m$  in [7] are as follows:

$$(4.10) \ M_m = \begin{cases} -\frac{R_1^2}{2} (\lambda^2 - 1) + h_1 \ln \lambda, & |m| = 1, \\ -\frac{R_1^{|m|+1}}{2} (\lambda^2 - 1) + \frac{h_m}{2(|m|-1)R_1^{|m|-1}} (1 - \lambda^{-2(|m|-1)}), & |m| > 1, \end{cases}$$

$$(4.11) N_m = R_1^{|m|} + \frac{h_m}{R_1^{|m|}} + \frac{2}{R_1} M_m, \quad |m| \ge 1,$$

with

(4.12)

$$h_{m} = \begin{cases} \frac{R_{1}^{2}}{2} \frac{(\lambda^{4} - 1)/2 + (\lambda^{2} - 1)}{\ln \lambda + (\lambda^{2} - 1)/2}, & |m| = 1, \\ R_{1}^{2|m|} \lambda^{2(|m|+1)} \frac{|m| - 1}{|m| + 1} \frac{1 + \lambda^{-2(|m|+1)} ((\lambda^{2} - 1)(|m| + 1) - 1)}{(\lambda^{2} - 1)(|m| - 1) + 1 - \lambda^{-2(|m|-1)}}, & |m| > 1, \end{cases}$$

and  $\lambda = R_2/R_1 > 1$ . Here  $R_2$  is the radius of the Stokes-Darcy domain  $\Omega$ .

*Proof.* Following the proof of Proposition 4.3 in [7] and using (4.3) and (4.6), we similarly obtain the modal coefficient  $S_m$  in (4.9).

Using the previous propositions, the iterative operator  $\mathcal{A} = \sum_{m \in \mathbf{Z}} \mathcal{A}_m H_m(\theta)$  can be written as follows:

(4.13) 
$$\mathcal{A}\eta = \sum_{m \in \mathbf{Z}} \begin{pmatrix} \mathcal{D}_m \eta_{p,m} \\ \mathcal{S}_m \eta_{f,m} \end{pmatrix} H_m(\theta) = \sum_{m \in \mathbf{Z}} \begin{pmatrix} 0 & \mathcal{D}_m \\ \mathcal{S}_m & 0 \end{pmatrix} \begin{pmatrix} \eta_{f,m} \\ \eta_{p,m} \end{pmatrix} H_m(\theta)$$

with

$$(4.14) \mathcal{A}_m := \begin{pmatrix} 0 & \mathcal{D}_m \\ \mathcal{S}_m & 0 \end{pmatrix} = \begin{pmatrix} 0 & \frac{\gamma_f K |m|/R_1 - 1}{\gamma_p M_m / \mu - N_m} \\ \frac{\gamma_p M_m / \mu - N_m}{\gamma_f M_m / \mu + N_m} & 0 \end{pmatrix}.$$

Before analyzing the convergence of the iteration operation by studying the coefficients  $A_m$ , we first provide the following asymptotic result needed in this analysis.

PROPOSITION 4.3. Let  $M_m$  and  $N_m$  be defined as in (4.10) and (4.11), respectively. Then, for |m| > 1, we have

$$\frac{N_m}{M_m} = \frac{2}{R_1} \left( 1 + (|m| - 1) \left( \frac{1}{\alpha_m} + \frac{\beta_m}{\alpha_m} \right) \right),$$

where

(4.16) 
$$\alpha_{m} = (1 - \lambda^{2-2|m|})\beta_{m} - (\lambda^{2} - 1)(|m| - 1),$$

$$\beta_{m} = \left(\frac{|m| - 1}{|m| + 1}\right) \frac{(\lambda^{2} - 1)(|m| + 1) - 1 + \lambda^{2|m| + 2}}{(\lambda^{2} - 1)(|m| - 1) + 1 - \lambda^{2-2|m|}}.$$

Moreover, we have

(4.17a) 
$$\frac{N_m}{M_m} = \frac{2}{R_1} |m| \left( 1 + O\left(\frac{|m|^2}{\lambda^{2|m|-2} - |m|^2}\right) \right),$$
(4.17b) 
$$\frac{N_2}{M_2} = \frac{2}{R_1} \left( 2 + \frac{4}{(\lambda^2 - 1)} + \frac{12}{(\lambda^2 - 1)^2} + \frac{12}{(\lambda^2 - 1)^3} \right),$$

and in particular,

$$\lim_{|m|\to +\infty}\frac{N_m}{M_m}=\frac{2}{R_1}|m|,\quad \lim_{\lambda\to +\infty}\frac{N_m}{M_m}=\frac{2}{R_1}|m|.$$

If |m| = 1, we have

(4.18) 
$$\frac{N_1}{M_1} = \frac{2}{R_1} \left( 1 + \frac{1}{\alpha_1} + \frac{\beta_1}{2\alpha_1} \right),$$

where  $\alpha_1 = \ln(\lambda)\beta_1 - (\lambda^2 - 1)$  and  $\beta_1 = \frac{(\lambda^2 + 3)(\lambda^2 - 1)}{2\ln(\lambda) + (\lambda^2 - 1)}$ . In addition, (4.19)

$$\frac{N_1}{M_1} = \frac{2}{R_1} \left( 1 + O\left(\frac{\lambda^2}{\ln(\lambda)\lambda^2 - (\lambda^2 - 1)}\right) \right), \text{ with } \lim_{\lambda \to +\infty} \frac{N_1}{M_1} = \frac{2}{R_1}, \lim_{\lambda \to 1^+} \frac{N_1}{M_1} = +\infty.$$

*Proof.* From the definitions of  $M_m$  and  $N_m$ , we can directly obtain (4.18) and (4.15) by symbolic calculations. It follows from the definitions of  $\alpha_1$  and  $\beta_1$  that (4.20)

$$\beta_1 = O\left(\frac{\lambda^2(\lambda^2 - 1)}{\lambda^2 - 1}\right) = O(\lambda^2), \quad \alpha_1 = \ln(\lambda)\beta_1 - (\lambda^2 - 1) = O(\ln(\lambda)\lambda^2 - (\lambda^2 - 1)).$$

Substituting (4.20) into (4.18), we have (4.19). Similarly,

(4.21)

$$\beta_m = O\left(\frac{|m|\lambda^{2|m|+2}}{(|m|+1)(\lambda^2-1)(|m|-1)}\right) = O\left(\frac{m\lambda^{2|m|+2}}{|m|^2\lambda^2-\lambda^2-|m|^2}\right) = O\left(\frac{\lambda^{2|m|}}{|m|}\right),$$
(4.22)

$$\alpha_m = O((1 - \lambda^{2-2|m|})\beta_m - (\lambda^2 - 1)(|m| - 1)) = O\left(\frac{\lambda^{2|m|}}{|m|} - \lambda^2|m|\right),$$

(4.23)

$$\frac{1}{\alpha_m} + \frac{\beta_m}{\alpha_m} = O\left(\frac{1 + \frac{\lambda^{2|m|}}{|m|}}{\frac{\lambda^{2|m|}}{|m|} - \lambda^2|m|}\right) = 1 + O\left(\frac{|m|^2}{\lambda^{2|m|-2} - |m|^2}\right).$$

Then we directly obtain (4.17a) from (4.23). Equation (4.17b) can be obtained by simple calculations.

THEOREM 4.4. Let  $\rho(A_m)$  be the spectral radius of  $A_m$  defined in (4.14). When  $\gamma_f = \gamma_p$ , we have

$$\rho(\mathcal{A}_0) = 1 \quad and \quad \rho(\mathcal{A}_m) < 1 \quad for \ m \neq 0.$$

*Proof.* It was proved in [7] that  $M_m > 0$  and  $N_m > 0$  for  $m \neq 0$ . It is easy then to see that  $|\mathcal{D}_m| < 1$  and  $|\mathcal{S}_m| < 1$  for  $\gamma_f = \gamma_p = \gamma$ . This implies in this case that  $|\mathcal{D}_m \mathcal{S}_m| < 1$ , and therefore,  $\rho(\mathcal{A}_m) < 1$  for  $m \neq 0$ . We can also proceed by setting  $C_m = \frac{M_m}{N_m}$  and use the definitions of  $D_m$  and  $S_m$  to obtain

$$\mathcal{D}_{m}\mathcal{S}_{m} = \frac{\gamma_{f}K|m|/R_{1} - 1}{\gamma_{p}K|m|/R_{1} + 1} \frac{\gamma_{p}C_{m}/\mu - 1}{\gamma_{f}C_{m}/\mu + 1}$$

$$= \frac{(\gamma_{f}\gamma_{p}|m|C_{m}K/(\mu R_{1}) + 1) - (\gamma_{f}K|m|/R_{1} + C_{m}\gamma_{p}/\mu)}{(\gamma_{f}\gamma_{p}|m|C_{m}K/(\mu R_{1}) + 1) + (\gamma_{p}K|m|/R_{1} + C_{m}\gamma_{f}/\mu)}$$

It is easy to find that  $|\mathcal{D}_m \mathcal{S}_m| < 1$  for  $\gamma_f = \gamma_p = \gamma$ , which means that  $\rho(\mathcal{A}_m) < 1$  for  $m \neq 0$ .

Because  $\rho(A_0) = 1$ , the iterative method may not converge. In this paper, we are interested in using a Krylov subspace method instead of the Jacobi type iterative method in order to avoid this constraint. Using (4.25), we obtain that

$$\lim_{|m| \to +\infty} \mathcal{D}_m \mathcal{S}_m = -\frac{\gamma_f}{\gamma_p}$$

which suggests that in order to have  $|\mathcal{D}_m \mathcal{S}_m| < 1$ , we need  $\gamma_f < \gamma_p$ . However, practically the solution is only represented by a finite number of modes m. The following corollary provides another approach in the choice of the parameters.

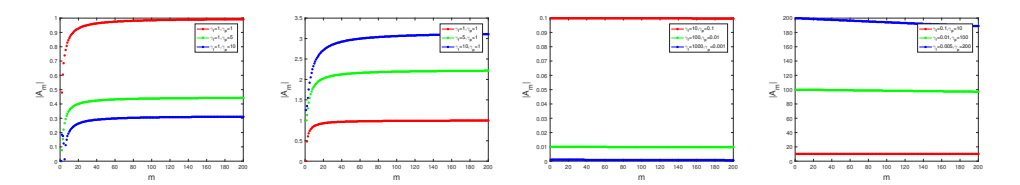


Fig. 3. Distribution of the spectral radius of  $A_m$  on different parameters  $\gamma_f, \gamma_p$ . Here  $K = 1, \mu = 1$  for the first two subfigures and  $K = 10^{-6}, \mu = 10^{-6}$  for the last two subfigures.

Corollary 4.5. By choosing  $\gamma_f$  and  $\gamma_p$  satisfying

(4.27) 
$$\gamma_f \gamma_p K/(2\mu) = 1$$
,  $\gamma_p K|m|/R_1 + C_m \gamma_f/\mu \gg \gamma_f K|m|/R_1 + C_m \gamma_p/\mu$ , we have  $|\rho(\mathcal{A}_m)| < 1$ .

*Proof.* If m is fixed, knowing that all the coefficients in (4.14) are positive and using (4.25), the result follows from the fact that in order to obtain a smaller spectral radius, we can choose  $\gamma_f$  and  $\gamma_p$  such that the term  $\gamma_p K |m|/R_1 + C_m \gamma_f / \mu$  is much larger than the term  $\gamma_f K |m|/R_1 + C_m \gamma_p / \mu$  and the term  $\gamma_f \gamma_p |m| C_m K / (\mu R_1)$  keeps moderate values. Using (4.17a), we find  $\gamma_f \gamma_p |m| C_m K / (\mu R_1) \lesssim \gamma_f \gamma_p K / (2\mu)$ . Therefore, we can set  $\gamma_f$  and  $\gamma_p$  to satisfy (4.27).

Remark 4.6. Figure 3 displays examples of the spectral radius with respect to different choices of  $\gamma_f$  and  $\gamma_p$  as well as different coefficients K and  $\mu$ . We can observe that the choice of  $\gamma_f$  and  $\gamma_p$  is crucial as it can lead to a very fast convergent or divergent iterative algorithm. Following the condition (4.27), we suggest the following settings in the choice of these parameters:

- For moderate  $\mu$  and K, set  $\gamma_f \leq \gamma_p$  with moderate  $\gamma_f$  and  $\gamma_p$ .
- For moderate  $\mu$  and small K, set  $\gamma_f \gg \gamma_p \geq 1$ .
- For small  $\mu$  and moderate K, set  $1 \geq \gamma_f \gg \gamma_p$ .
- For small  $\mu$  and K, set  $\gamma_f \gg \gamma_p, \gamma_f \geq 1, \gamma_p \leq 1$ .

From the above settings, we can see that when K or  $\mu$  is small, to obtain  $|\mathcal{A}_m| \leq 1$ , we need  $\gamma_f \geq \gamma_p$ . However, when K and  $\mu$  are moderate, the condition  $\gamma_f \leq \gamma_p$  is necessary. The results coincide with the theoretical and numerical results in [9]. To verify the above choices for parameters, in Figure 3 we show some choices of parameters satisfying or not satisfying the above settings. The results validate the above settings.

Remark 4.7. From the expansion form (4.17a), we know that  $N_m/M_m$  exponentially approximates  $2|m|/R_1$ , which is shown in Figure 4. When  $\lambda$  is moderate, there are few points far away from the asymptote, which means that the simple approximation  $2|m|/R_1$  is a good substitute for  $N_m/M_m$  for almost every mode.

Remark 4.8. It is interesting to further understand the connections and differences between this paper and two important related works [7, 17]. First, while we follow a local operator idea in this paper, there are also some nonlocal operator ideas in the literature. For example, if  $\gamma_f = \frac{R_1}{K|m|}$  and  $\gamma_p = \frac{\mu N_m}{M_m}$  are chosen in (4.14), we have  $\mathcal{A}_m = 0$ , which implies the optimal convergence. However, this idea leads  $\gamma_f$  and  $\gamma_p$  to be nonlocal operators (see [7] for more about nonlocal operators). On the other hand, using (4.17a), we find that

(4.28) 
$$\gamma_f \gamma_p = \frac{R_1 \mu}{K} \frac{N_m}{|m| M_m} \approx \frac{2\mu}{K},$$

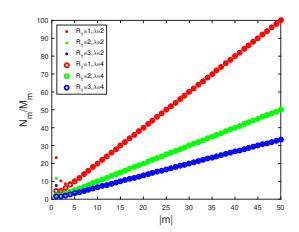


Fig. 4. Change of  $\frac{N_m}{M_m}$  with respect to m for different  $R_1$  and  $\lambda$ .

which is consistent with the hyperbolic relation in [17]. This relation was utilized in [17] to derive the parameter optimization, whose conclusions will be recalled in subsection 5.1. In this paper, our idea is to develop the linear relation for deriving the parameter optimization in subsection 5.2.

5. Optimal Robin parameters. Although Corollary 4.5 can provide an effective strategy in the choice of the Robin parameters, it is still possible to use optimization methods to optimize these parameters for a better convergence in the case of many practical situations.

In this section, we describe how to achieve optimal Robin parameters from the explicit form of the iteration operator. Without loss of generality, we consider continuous m with the case of m>0 in the following analysis. Denote the spectral radius by  $\rho(\gamma_f, \gamma_p, m) = |D_m S_m| := |\bar{g}(\gamma_f, \gamma_p, m)|$ , where

(5.1) 
$$\bar{g}(\gamma_f, \gamma_p, m) = \left(\frac{\gamma_f K m / R_1 - 1}{\gamma_p K m / R_1 + 1}\right) \left(\frac{\gamma_p C_m / \mu - 1}{\gamma_f C_m / \mu + 1}\right).$$

Our analysis of the rate (5.1) consists of finding optimal coefficients  $\gamma_p$  and  $\gamma_f$  in order to improve the convergence using Krylov methods. As we can see, the rate of convergence (5.1) is composed of two terms related to Darcy and Stokes problems, and the latter is given in function of the quantity  $C_m$  which is technically difficult to manipulate. For this reason, we propose using the expansion of  $C_m$  for large m. Recall that  $C_m = M_m/N_m$ , where  $M_m$ ,  $N_m$  are defined by (4.10) and (4.11) and the expansion for large m is computed for  $N_m/M_m$ . On the other hand, our goal is to design an improved algorithm for each mode. Therefore, in the following we investigate the effects on this change mode by mode, by numerically studying

(5.2) 
$$\mathcal{E}(m) = \frac{N_m}{M_m} - \frac{2m}{R_1}.$$

We also note that  $\mathcal{E}(m) = 0$  if

(5.3) 
$$\frac{1}{\alpha_m} + \frac{\beta_m}{\alpha_m} = 1 \quad (m > 1), \quad \frac{1}{\alpha_1} + \frac{\beta_1}{2\alpha_1} = 0 \quad (m = 1),$$

where  $\alpha_m, \beta_m$  and  $\alpha_1, \beta_1$  are defined in Proposition 4.3. Denote  $e(m) = (\frac{1}{\alpha_m} + \frac{\beta_m}{\alpha_m}) - 1$ , m > 1, and  $e(1) = \frac{1}{\alpha_1} + \frac{\beta_1}{2\alpha_1}$ . Using Proposition 4.3 and some simple computation, (5.3) is nearly satisfied as

$$e(m) = \frac{m^2(m-1)\lambda^{2m+4} - (2m-4)(m^2-1)\lambda^{2m+2} + (m^3 - 3m + 4)\lambda^{2m} - 2m\lambda^2}{(m-1)(\lambda^{4m+2} - m^2\lambda^{2m+4} + 2(m^2 - 1)\lambda^{2m+2} - m^2\lambda^{2m})}$$

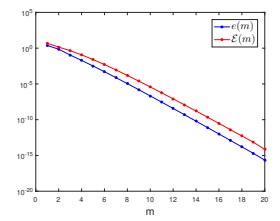


Fig. 5. Effect of the negligible part of  $N_m/M_m$  with respect to m.

$$\approx \frac{m^2}{\lambda^{2m-2}-m^2}, \ m>1,$$

which decays exponentially with mode m; see Figure 5. However, even if  $\mathcal{E}(m)$  or e(m) is not very well approximated at the first few modes, the effective convergence of the algorithm will not be affected when using Krylov subspace methods to deal with the iteration operator.

Using the approximation mentioned in Remark 4.7 and shown in Figure 4, the rate of convergence (5.1) becomes

(5.4) 
$$g(\gamma_f, \gamma_p, m) = \left(\frac{2\widetilde{\mu}m - \gamma_p}{2\widetilde{\mu}m + \gamma_f}\right) \left(\frac{1 - \gamma_f \widetilde{K}m}{1 + \gamma_p \widetilde{K}m}\right) \approx \bar{g}(\gamma_f, \gamma_p, m),$$

where  $\widetilde{\mu} = \mu/R_1$  and  $\widetilde{K} = K/R_1$ . Generally speaking, writing  $g(\gamma_f, \gamma_p, m) = D_m S_m$ , we can observe that  $|D_m| < 1$  (resp.,  $|S_m| < 1$ ) if  $\gamma_f < \gamma_p$  (resp.,  $\gamma_p < \gamma_f$ ). We will see that the proposed method has an improved rate compared with the one proposed in [14] where  $\gamma_f = \gamma_p$ .

Note that the spectral radius  $\rho = |g(\gamma_f, \gamma_p, m)|$  in (5.4) is similar to the reduction factor in [17], where three methods of optimization were introduced including the Taylor approximation, the classical min-max, and the minimization approaches for the expectation of the reduction factor. The last two optimization techniques are based on the hyperbolic relation of Robin parameters in (4.28). In the rest of this section, we review this method and then present the new one based on a linear relation. Following [17], we consider the interval  $[m_{\min}, m_{\max}]$  of mode m where the lowest mode  $m_{\min} = \pi/L$  (L being the length of the interface  $\Gamma$ ). On the other hand, for the discrete mesh size h of  $\Omega$  in the numerical implementation, we set the highest mode  $m_{\max} = \pi/h$  following the references [17, 29].

- **5.1. Hyperbolic relation.** In this subsection, we review and explain the two optimization techniques mentioned above, based on the hyperbolic relation  $\gamma_f \gamma_p = \frac{2\tilde{\mu}}{\tilde{K}}$ , which has been discussed in detail in [17].
- **5.1.1. The classical min-max approach.** This approach consists of finding  $\gamma_f$  and  $\gamma_p$  satisfying the hyperbolic relation such that the Robin parameters minimize the spectral radius over all the relevant modes m. We recall the following proposition from [17].

Proposition 5.1. The solution of the min-max problem

$$\min_{\gamma_f \gamma_p = \frac{2\tilde{\mu}}{K}} \max_{m \in [m_{\min}, m_{\max}]} \rho(\gamma_f, \gamma_p, m) = \min_{\gamma_f \gamma_p = \frac{2\tilde{\mu}}{K}} \max \left\{ \rho(\gamma_f, \gamma_p, m_{\min}), \rho(\gamma_f, \gamma_p, m_{\max}) \right\}$$

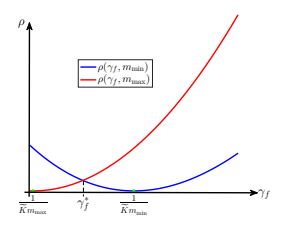


Fig. 6. Change of the spectral radius with respect to  $\gamma_f$  for the hyperbolic relation case.

is given by the pair

$$\begin{split} \gamma_f^* &= \frac{1 - 2\widetilde{\mu}\widetilde{K}m_{\min}m_{\max}}{\widetilde{K}(m_{\min} + m_{\max})} + \sqrt{\left(\frac{1 - 2\widetilde{\mu}\widetilde{K}m_{\min}m_{\max}}{\widetilde{K}(m_{\min} + m_{\max})}\right)^2 + \frac{2\widetilde{\mu}}{\widetilde{K}}}, \\ \gamma_p^* &= -\frac{1 - 2\widetilde{\mu}\widetilde{K}m_{\min}m_{\max}}{\widetilde{K}(m_{\min} + m_{\max})} + \sqrt{\left(\frac{1 - 2\widetilde{\mu}\widetilde{K}m_{\min}m_{\max}}{\widetilde{K}(m_{\min} + m_{\max})}\right)^2 + \frac{2\widetilde{\mu}}{\widetilde{K}}}. \end{split}$$

Moreover,  $\rho(\gamma_f^*, \gamma_p^*, m) < 1$  for all  $m \in [m_{\min}, m_{\max}]$ .

Remark 5.2. From the proof of Proposition 3.3 in [17], we can find that

$$\rho(\gamma_f, m) := \rho(\gamma_f, \gamma_p, m)|_{\gamma_f \gamma_p = \frac{2\widetilde{\mu}}{\widetilde{K}}} = \frac{2\widetilde{\mu}}{\widetilde{K}} \left(\frac{\widetilde{K}\gamma_f m - 1}{2\widetilde{\mu}m + \gamma_f}\right)^2$$

is always positive, decreasing for  $\gamma_f < \frac{1}{\widetilde{K}m}$  and increasing for  $\gamma_f \geq \frac{1}{\widetilde{K}m}$ . Therefore, we can obtain that  $\gamma_f^* \in [\frac{1}{\widetilde{K}m_{\max}}, \frac{1}{\widetilde{K}m_{\min}}]$ ; see Figure 6. Particularly, for the optimal parameter pair  $(\gamma_f^*, \gamma_p^*)$ , the spectral radii of  $m_{\min}$  and  $m_{\max}$  are equal, i.e.,  $\rho(\gamma_f^*, \gamma_p^*, m_{\min}) = \rho(\gamma_f^*, \gamma_p^*, m_{\max})$ .

**5.1.2.** Minimization of the spectral expectation. As discussed in [17], the min-max approach does not necessarily lead to the fastest convergence of Krylov methods. Therefore, in [17] the authors further consider the minimization approach of the spectral expectation, which is to find  $\gamma_f$  and  $\gamma_p$  satisfying the hyperbolic relation such that the Robin parameters minimize the expectation  $E(\gamma_f, \gamma_p)$  of  $\rho(\gamma_f, \gamma_p, m)$  on the set  $\mathcal{A}_f = \{ \gamma_f > 0 : \rho(\gamma_f, \gamma_p, m) \mid_{\gamma_f \gamma_p = \frac{2\tilde{\mu}}{K}} \leq 1 \,\forall m \in [m_{\min}, m_{\max}] \}$ :

(5.6) 
$$\min_{\substack{\gamma_f \in A_f \\ \gamma_f \gamma_p = \frac{2\tilde{\mu}}{\tilde{K}}}} E(\gamma_f, \gamma_p) := \min_{\gamma_f \in A_f} E(\gamma_f),$$

where

$$\begin{split} E(\gamma_f) &= E(\gamma_f, \gamma_p)|_{\gamma_f \gamma_p = \frac{2\widetilde{\mu}}{\widetilde{K}}} = \frac{1}{m_{\max} - m_{\min}} \int_{m_{\min}}^{m_{\max}} \rho(\gamma_f, \gamma_p, m) \mathrm{d}m \\ &= \frac{\gamma_f^2 \widetilde{K}}{2\widetilde{\mu}} + \frac{(\gamma_f^2 \widetilde{K} + 2\widetilde{\mu})^2}{2\widetilde{\mu} \widetilde{K} (2\widetilde{\mu} m_{\max} + \gamma_f) (2\widetilde{\mu} m_{\min} + \gamma_f)} \\ &- \frac{\gamma_f (\gamma_f^2 \widetilde{K} + 2\widetilde{\mu})}{2\widetilde{\mu}^2 (m_{\max} - m_{\min})} \ln \left( \frac{2\widetilde{\mu} m_{\max} + \gamma_f}{2\widetilde{\mu} m_{\min} + \gamma_f} \right). \end{split}$$

From Lemma 3.5 of [17], the set  $\mathcal{A}_f$  has no upper bound for some cases. We note that the solution of the minimization problem (5.6) with  $\mathcal{A}_f$  is equivalent to that with  $\mathcal{A}_f^* := \mathcal{A}_f \cap (0, \frac{1}{\widetilde{K}m_{\min}}]$ . In fact, let  $\partial_{\gamma_f} E(1/(\widetilde{K}m)) := N(m)/D(m)$ ; then we can derive

$$\begin{split} D(m) &= -2\widetilde{\mu}^2 \widetilde{K} (2\widetilde{\mu} m_{\min} + 1/(\widetilde{K} m))^2 (2\widetilde{\mu} m_{\max} + 1/(\widetilde{K} m))^2 (m_{\max} - m_{\min}) < 0, \\ N(m) &= \left( 8\widetilde{\mu}^4 (m_{\max}^2 - m_{\min}^2) + \frac{8\widetilde{\mu}^3}{\widetilde{K} m} (m_{\max} - m_{\min}) + \frac{4\widetilde{\mu}^2}{\widetilde{K}^2 m^3} (m_{\max} - m_{\min}) \right) \\ &+ \left( \frac{32\widetilde{\mu}^4 m_{\min} m_{\max}}{m^2} (m_{\min}^2 - m_{\max}^2) + \frac{8\widetilde{\mu}^3}{\widetilde{K} m^3} (m_{\min}^3 - m_{\max}^3) \right) \\ &+ \frac{10\widetilde{\mu}^2}{\widetilde{K}^2 m^4} (m_{\min}^2 - m_{\max}^2) \right) + N_r(m) \\ &< 8\widetilde{\mu}^4 (m_{\min}^2 - m_{\max}^2) \left( \frac{4m_{\min} m_{\max}}{m^2} - 1 \right) \\ &+ \frac{8\widetilde{\mu}^3}{\widetilde{K} m} (m_{\min} - m_{\max}) \left( \frac{m_{\min}^2 + m_{\max}^2 + m_{\min} m_{\max}}{m^2} - 1 \right) \\ &+ \frac{2\widetilde{\mu}^2}{\widetilde{K}^2 m^3} (m_{\min} - m_{\max}) \left( \frac{5(m_{\min} + m_{\max})}{m} - 2 \right), \end{split}$$

where  $N_r(m)$  is the remaining part of N(m) consisting of some negative algebraic expressions. Particularly N(m) < 0 when  $m \le m_{\min}$ . Hence, we have  $\partial_{\gamma_f} E(\gamma_f) > 0$  for any  $\gamma_f \ge 1/(\widetilde{K}m_{\min})$ .

Due to the complex algebra expression of  $E(\gamma_f)$ , we consider a simple numerical approximation  $\gamma_f^*$ , instead of the analytical optimal parameter  $\gamma_f$ , following the steps:

- 1. Divide the interval  $\mathcal{A}_f^*$  into n equal subintervals and denote the point set by  $\{\gamma_f^i\}_{i=0}^n$ .
- 2. For each point  $\gamma_f^i$ , compute  $E(\gamma_f^i)$ .
- 3. Find the index  $s \in \{0, \dots, n\}$  such that  $E(\gamma_f^s)$  is the minimum of  $\{E(\gamma_f^i)\}_{i=0}^n$  and set  $\gamma_f^* = \gamma_f^s$ .

Remark 5.3. In [17], the restriction  $\mathcal{A}_f$  is used. In this paper, we propose replacing  $\mathcal{A}_f^*$  by a simpler  $\mathcal{I}_f$ , which will be defined in the following subsection.

**5.2. Linear relation.** The hyperbolic relation is not the only choice for selecting the Robin parameters. From Figure 5 in [17], we can see that any curve connecting the two end points of the hyperbola can also cut off all the contour lines. In this section, we introduce a simple and effective linear relation for an alternative optimization technique of the Robin parameters. These parameters  $(\gamma_f \text{ and } \gamma_p)$  are then computed using the classical min-max and the minimization of the spectral expectation methods. From the expression of  $g(\gamma_f, \gamma_p, m)$ , we note that for the extreme points  $m_{\min}$  and  $m_{\max}$ , the parameters pairs  $(\gamma_f, \gamma_p)$  reach optima (i.e.,  $\rho = 0$ ) at  $(\frac{1}{\widetilde{K}m_{\min}}, 2\widetilde{\mu}m_{\min})$  and  $(\frac{1}{\widetilde{K}m_{\max}}, 2\widetilde{\mu}m_{\max})$ , respectively. Hence the linear relation we propose is as follows:

(5.7) 
$$\gamma_p = \left(-2\widetilde{\mu}\widetilde{K}m_{\min}m_{\max}\right)\gamma_f + 2\widetilde{\mu}(m_{\min} + m_{\max}) := p\gamma_f + q, \quad \gamma_f \in \mathcal{I}_f,$$

where  $\mathcal{I}_f = \left[\frac{1}{\widetilde{K}m_{\max}}, \frac{1}{\widetilde{K}m_{\min}}\right]$ . To simplify the following discussions, we define the notation  $\bar{m} = \frac{1}{2}(m_{\min} + m_{\max})$  and  $\widehat{m} = m_{\min}m_{\max}$ .

**5.2.1. The classical min-max approach.** First, we obtain the following basic conclusion for the min-max approach with the linear relation.

Proposition 5.4. Let  $(\gamma_f^{\star}, \gamma_p^{\star})$  be the solution of the min-max problem

(5.8) 
$$\min_{\gamma_p = p\gamma_f + q} \max_{m \in [m_{\min}, m_{\max}]} \rho(\gamma_f, \gamma_p, m) \\ = \min_{\gamma_p = p\gamma_f + q} \max \left\{ \rho(\gamma_f, \gamma_p, m_{\min}), \rho(\gamma_f, \gamma_p, m_{\max}), \rho(\gamma_f, \gamma_p, m_c) \right\}.$$

Then  $\rho(\gamma_f^{\star}, \gamma_p^{\star}, m) < 1$  for all  $m \in [m_{\min}, m_{\max}]$ . Here

(5.9) 
$$m_c = \frac{\sqrt{2\widetilde{\mu}\widetilde{K}(2\widetilde{\mu} + \widetilde{K}\gamma_f^2)(2\widetilde{\mu} + \widetilde{K}\gamma_p^2)} + 2\widetilde{\mu}\widetilde{K}(\gamma_p - \gamma_f)}{2\widetilde{\mu}\widetilde{K}(2\widetilde{\mu} + \gamma_f\gamma_p\widetilde{K})},$$

$$m_c \in [m_{1c}, m_{2c}], \ m_{1c} = \frac{1}{\gamma_f \widetilde{K}}, \ and \ m_{2c} = \frac{\gamma_p}{2\widetilde{\mu}} = 2\bar{m} - \gamma_f \widetilde{K} \widehat{m}.$$

*Proof.* From the definition  $\rho(\gamma_f, \gamma_p, m) = |g(\gamma_f, \gamma_p, m)|$ , we know that the spectral radius is always positive and has two minimums  $(\rho = 0)$  at  $m = m_{1c}$  and  $m = m_{2c}$ . Due to its continuity, the maximum is obtained at one of  $\{m_{\min}, m_{\max}, m_c\}$ , where  $m_c \in [m_{1c}, m_{2c}]$  is a local maximum. In fact, on the interval  $[m_{1c}, m_{2c}]$ , we have

$$\rho(\gamma_f, \gamma_p, m) = \left(\frac{\gamma_p - 2\widetilde{\mu}m}{2\widetilde{\mu}m + \gamma_f}\right) \cdot \left(\frac{\gamma_f \widetilde{K}m - 1}{1 + \gamma_p \widetilde{K}m}\right),$$

and then solve the equation  $\partial_m \rho(\gamma_f, \gamma_p, m) = 0$  resulting in (5.9). For the result  $m_c \in [m_{1c}, m_{2c}]$ , it is actually based on the fact  $\gamma_f \gamma_p \geq \frac{2\tilde{\mu}}{\tilde{K}}$  on the straight segment (5.7). First,  $m_c \geq m_{1c}$  is equivalent to

$$2\widetilde{\mu}(2\widetilde{\mu} + \gamma_f \gamma_p \widetilde{K}) - 2\widetilde{\mu}\widetilde{K}\gamma_f(\gamma_p - \gamma_f) \le \gamma_f \sqrt{2\widetilde{\mu}\widetilde{K}(2\widetilde{\mu} + \widetilde{K}\gamma_f^2)(2\widetilde{\mu} + \widetilde{K}\gamma_p^2)}.$$

That is,

$$2\widetilde{\mu}(2\widetilde{\mu} + \widetilde{K}\gamma_f^2) \le \gamma_f \sqrt{2\widetilde{\mu}\widetilde{K}(2\widetilde{\mu} + \widetilde{K}\gamma_f^2)(2\widetilde{\mu} + \widetilde{K}\gamma_p^2)},$$

which holds provided

(5.10) 
$$2\widetilde{\mu}(2\widetilde{\mu} + \widetilde{K}\gamma_f^2) \le \gamma_f^2 \widetilde{K}(2\widetilde{\mu} + \widetilde{K}\gamma_p^2).$$

The inequality (5.10) is obtained from the fact  $\gamma_f \gamma_p \geq \frac{2\tilde{\mu}}{\tilde{K}}$ . Similarly, we have  $m_c \leq m_{2c}$ .

To prove the inequality  $\rho(\gamma_f^{\star}, \gamma_p^{\star}, m) < 1$  holding for any  $m \in [m_{\min}, m_{\max}]$ , we define  $(\gamma_f^{\circ}, \gamma_p^{\circ})$  as follows:

$$\gamma_f^{\circ} = \frac{\frac{1}{\widetilde{K}m_{\max}} + \frac{1}{\widetilde{K}m_{\min}}}{2} = \frac{\bar{m}}{\widetilde{K}\widehat{m}} \in \mathcal{I}_f, \quad \gamma_p^{\circ} = p\gamma_f^{\circ} + q = 2\widetilde{\mu}\bar{m}.$$

Then the parameter pair  $(\gamma_f^{\circ}, \gamma_p^{\circ})$  satisfies the linear relation on the interval  $\mathcal{I}_f$ , which means  $\rho(\gamma_f^{\star}, \gamma_p^{\star}, m) \leq \rho(\gamma_f^{\circ}, \gamma_p^{\circ}, m)$ . Now we just need to prove a stronger inequality,  $\rho(\gamma_f^{\circ}, \gamma_p^{\circ}, m) < 1$ , holding for any  $m \in [m_{\min}, m_{\max}]$  or equivalently for  $m \in \{m_{\min}, m_{\max}, m_c\}$ . Set  $m = m_{\min}$ ; then

$$(5.11) \ \rho(\gamma_f^{\circ}, \gamma_p^{\circ}, m_{\min}) = \left(\frac{2\widetilde{\mu}\bar{m} - 2\widetilde{\mu}m_{\min}}{2\widetilde{\mu}m_{\min} + \frac{\bar{m}}{\widetilde{K}\widehat{m}}}\right) \cdot \left(\frac{1 - \widetilde{K}m_{\min}\frac{\bar{m}}{\widetilde{K}\widehat{m}}}{1 + 2\widetilde{K}\widetilde{\mu}m_{\min}\bar{m}}\right)$$

$$=\frac{\widetilde{K}\widetilde{\mu}m_{\min}(m_{\max}-m_{\min})^2}{\left(4\widetilde{K}\widetilde{\mu}m_{\min}\widehat{m}+2\bar{m}\right)\left(1+2\widetilde{K}\widetilde{\mu}m_{\min}\bar{m}\right)}<\frac{\widetilde{K}\widetilde{\mu}m_{\min}(m_{\max}-m_{\min})^2}{4\widetilde{K}\widetilde{\mu}m_{\min}\bar{m}^2}<1.$$

For  $m = m_{\text{max}}$ , we have

(5.12)

$$\begin{split} &\rho(\gamma_f^{\circ},\gamma_p^{\circ},m_{\max}) = \left(\frac{2\widetilde{\mu}m_{\max}-2\widetilde{\mu}\bar{m}}{2\widetilde{\mu}m_{\max}+\frac{\bar{m}}{\widetilde{K}\widehat{m}}}\right) \cdot \left(\frac{\widetilde{K}m_{\max}\frac{\bar{m}}{\widetilde{K}\widehat{m}}-1}{1+2\widetilde{K}\widetilde{\mu}m_{\max}\bar{m}}\right) \\ &= \frac{\widetilde{K}\widetilde{\mu}m_{\max}(m_{\max}-m_{\min})^2}{\left(4\widetilde{K}\widetilde{\mu}m_{\max}\widehat{m}+2\bar{m}\right)\left(1+2\widetilde{K}\widetilde{\mu}m_{\max}\bar{m}\right)} < \frac{\widetilde{K}\widetilde{\mu}m_{\max}(m_{\max}-m_{\min})^2}{4\widetilde{K}\widetilde{\mu}m_{\max}\bar{m}^2} < 1. \end{split}$$

Let  $m = m_c$ . Using the facts

$$2\widetilde{\mu}\overline{m} - 2\widetilde{\mu}m_c \le 2\widetilde{\mu}\overline{m} - 2\widetilde{\mu}m_{\min} = \widetilde{\mu}(m_{\max} - m_{\min}),$$

$$2\widetilde{K}m_c\overline{m} - 2\widetilde{K}\widehat{m} \le 2\widetilde{K}m_c\overline{m} - 2\widetilde{K}m_{\min}m_c = \widetilde{K}m_c(m_{\max} - m_{\min}),$$

we obtain

$$(5.13) \ \rho(\gamma_f^{\circ}, \gamma_p^{\circ}, m_c) = \left(\frac{2\widetilde{\mu}\overline{m} - 2\widetilde{\mu}m_c}{2\widetilde{\mu}m_c + \frac{\widetilde{m}}{\widetilde{K}\widehat{m}}}\right) \cdot \left(\frac{\widetilde{K}m_c \frac{\widetilde{m}}{\widetilde{K}\widehat{m}} - 1}{1 + 2\widetilde{K}\widetilde{\mu}m_c\overline{m}}\right)$$

$$< \frac{(\widetilde{\mu}(m_{\max} - m_{\min}))\left(\widetilde{K}m_c(m_{\max} - m_{\min})\right)}{\left(4\widetilde{K}\widetilde{\mu}m_c\widehat{m} + 2\overline{m}\right)\left(1 + 2\widetilde{K}\widetilde{\mu}m_c\overline{m}\right)} < \frac{\widetilde{K}\widetilde{\mu}m_c(m_{\max} - m_{\min})^2}{4\widetilde{K}\widetilde{\mu}m_c\overline{m}^2} < 1.$$

Then we complete the proof from (5.11)–(5.13)

Remark 5.5. It is difficult to explicitly obtain the optimal parameter using the min-max method with linear relation. Therefore, one efficient numerical implementation can be considered as follows:

- 1. Divide the interval  $\mathcal{I}_f$  into n equal subintervals and denote the node set by  $\begin{aligned} \left\{ \gamma_f^i \right\}_{i=0}^n. \\ \text{2. For each node } \gamma_f^i, \text{ compute} \end{aligned}$

$$\rho_{\max}^i = \max\left\{\rho(\gamma_f^i, \gamma_p^i, m_{\min}), \rho(\gamma_f^i, \gamma_p^i, m_{\max}), \rho(\gamma_f^i, \gamma_p^i, m_c)\right\},$$

where  $\gamma_p^i = p\gamma_f^i + q$ .

3. Find the index  $s \in \{0, \dots, n\}$  such that  $\rho_{\max}^s$  is the minimum of  $\{\rho_{\max}^i\}_{i=0}^n$  and then set  $\gamma_f^\star = \gamma_f^s$ .

LEMMA 5.6. Let  $(\gamma_f^*, \gamma_p^*)$  be the solution of the problem (5.5), and let  $(\gamma_f^o, \gamma_p^o)$  be the intersection point of two lines  $\gamma_p = p\gamma_f + q$  and  $\gamma_p = \frac{\gamma_p^*}{\gamma_f^*}\gamma_f$  (see Figure 7). Then

$$(5.14) \qquad \rho(\gamma_f^*, \gamma_p^*, m_{\min}) > \rho(\gamma_f^o, \gamma_p^o, m_{\min}), \quad \rho(\gamma_f^*, \gamma_p^*, m_{\max}) > \rho(\gamma_f^o, \gamma_p^o, m_{\max}).$$

*Proof.* From the definition and the hyperbolic relation of  $(\gamma_f^*, \gamma_p^*)$ , we have

$$\rho(\gamma_f^*, \gamma_p^*, m) = \frac{2\widetilde{\mu}}{\widetilde{K}} \left( \frac{\widetilde{K} \gamma_f^* m - 1}{2\widetilde{\mu} m + \gamma_f^*} \right)^2 := \frac{2\widetilde{\mu}}{\widetilde{K}} \frac{a_1(m)}{b_1(m)},$$

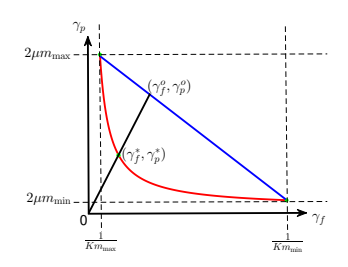


Fig. 7. Relationship of  $(\gamma_f^*, \gamma_p^*)$  and  $(\gamma_f^o, \gamma_p^o)$ .

where  $a_1(m) = (\widetilde{K}\gamma_f^*m)^2 - 2\widetilde{K}\gamma_f^*m + 1$  and  $b_1(m) = (2\widetilde{\mu}m)^2 + 4\widetilde{\mu}m\gamma_f^* + (\gamma_f^*)^2$  are positive for all m in  $[m_{\min}, m_{\max}]$ . From [17], it was found that  $\rho(\gamma_f^*, \gamma_p^*, m_{\min}) = \rho(\gamma_f^*, \gamma_p^*, m_{\max})$ . Using the definition of  $(\gamma_f^o, \gamma_p^o)$ , we have  $\gamma_f^* < \gamma_f^o$  and

$$\gamma_f^o = \frac{2\widetilde{K}(\gamma_f^*)^2 \bar{m}}{1 + \widetilde{K}^2(\gamma_f^*)^2 \widehat{m}}, \quad \gamma_p^o = \frac{2\widetilde{\mu}}{\widetilde{K}(\gamma_f^*)^2} \gamma_f^o,$$

which follow that

$$\rho(\gamma_f^o,\gamma_p^o,m) = \frac{2\widetilde{\mu}}{\widetilde{K}} \left( \frac{\widetilde{K}\gamma_f^*m - \frac{\gamma_f^o}{\gamma_f^*}}{2\widetilde{\mu}m\frac{\gamma_f^o}{\gamma_f^*} + \gamma_f^*} \right) \left( \frac{\widetilde{K}\gamma_f^om - 1}{2\widetilde{\mu}m + \gamma_f^o} \right) := \frac{2\widetilde{\mu}}{\widetilde{K}} \frac{a_2(m)}{b_2(m)}, \quad m \in \{m_{\min}, m_{\max}\} \,,$$

where  $a_2(m) = \widetilde{K}^2 \gamma_f^* \gamma_f^o m^2 - \widetilde{K} m (\gamma_f^* + \frac{(\gamma_f^o)^2}{\gamma_f^*}) + \frac{\gamma_f^o}{\gamma_f^*}$  and  $b_2(m) = (2\widetilde{\mu}m)^2 \frac{\gamma_f^o}{\gamma_f^*} + 2\widetilde{\mu} m (\gamma_f^* + \frac{(\gamma_f^o)^2}{\gamma_f^*}) + \gamma_f^* \gamma_f^o$  are positive for  $m \in \{m_{\min}, m_{\max}\}$ . By the definitions of  $a_1(m), b_1(m)$ , and  $a_2(m), b_2(m)$ , we have

$$a_{1}(m)b_{2}(m) - a_{2}(m)b_{1}(m) = (\widetilde{K}m)^{2}(2\widetilde{\mu}m)\gamma_{f}^{*}(\gamma_{f}^{*} - \gamma_{f}^{o})^{2} + 2\widetilde{\mu}m\left(\gamma_{f}^{*} + \frac{(\gamma_{f}^{o})^{2}}{\gamma_{f}^{*}} - 2\gamma_{f}^{o}\right) + \widetilde{K}m(2\widetilde{\mu}m)^{2}\left(\gamma_{f}^{*} + \frac{(\gamma_{f}^{o})^{2}}{\gamma_{f}^{*}} - 2\gamma_{f}^{o}\right) + \widetilde{K}m\gamma_{f}^{*}(\gamma_{f}^{*} - \gamma_{f}^{o}) > 0, \quad m \in \{m_{\min}, m_{\max}\},$$

which means that the inequalities in (5.14) hold.

LEMMA 5.7. Let  $(\gamma_f^*, \gamma_p^*)$  and  $(\gamma_f^o, \gamma_p^o)$  be defined as in Lemma 5.6. Then

(5.15) 
$$\lim_{\widetilde{K}\to 0} \gamma_f^* = \frac{1}{\widetilde{K}\bar{m}}, \quad \lim_{\widetilde{K}\to 0} \frac{a_1(m_{\max})}{b_1(m_{\max})} = \left(\frac{\widetilde{K}(m_{\max} - m_{\min})}{2}\right)^2,$$

(5.16) 
$$\lim_{\widetilde{K}\to 0} \gamma_f^o = \frac{2\bar{m}}{\widetilde{K}(\bar{m}^2 + \widehat{m})}, \quad \lim_{\widetilde{K}\to 0} \gamma_p^o = \frac{4\widetilde{\mu}\bar{m}^3}{\bar{m}^2 + \widehat{m}},$$

(5.17) 
$$\lim_{\widetilde{K} \to 0} m_c(\gamma_f^o, \gamma_p^o) = \frac{(\bar{m}^2 + \hat{m})^2 + 4\bar{m}^4}{4\bar{m}(\bar{m}^2 + \hat{m})}.$$

*Proof.* Using the Taylor expansion, we can easily obtain the limit of  $\gamma_f^*$ . Then using the limit of  $\gamma_f^*$ , we can deduce (5.15) and (5.16). Based on (5.15) and (5.16),

from the definition of  $m_c$ , we have

$$\lim_{\widetilde{K}\to 0} m_c(\gamma_f^o, \gamma_p^o) = \lim_{\widetilde{K}\to 0} \frac{\sqrt{(2\widetilde{\mu}\widetilde{K}\gamma_f^o)^2 + 2\widetilde{\mu}\widetilde{K}\left((2\widetilde{\mu})^2 + (\gamma_f^o\gamma_p^o\widetilde{K})^2\right)} + 2\widetilde{\mu}\widetilde{K}(\gamma_p^o - \gamma_f^o)}{2\widetilde{\mu}\widetilde{K}(2\widetilde{\mu} + \gamma_f^o\gamma_p^o\widetilde{K})}$$

$$= \lim_{\widetilde{K}\to 0} \frac{1}{2} \left(\frac{2\widetilde{\mu} + \widetilde{K}\gamma_f^o\gamma_p^o}{2\widetilde{\mu}\widetilde{K}\gamma_f^o}\right) = \frac{\left(\overline{m}^2 + \widehat{m}\right)^2 + 4\overline{m}^4}{4\overline{m}\left(\overline{m}^2 + \widehat{m}\right)}.$$

From Lemma 5.7, we know that  $\rho(\gamma_f^*, \gamma_p^*, m)$  converges to zero and  $m_c(\gamma_f^o, \gamma_p^o)$  converges to a constant when  $\widetilde{K}$  tends to zero. For the special parameter pair  $(\gamma_f^o, \gamma_p^o)$ , we can see from the asymptotic expression that  $\gamma_f^o$  is proportional to  $\frac{1}{\widetilde{K}}$  but  $\gamma_p^o$  is proportional to  $\widetilde{\mu}$  when  $\widetilde{K}$  tends to zero.

LEMMA 5.8. Let  $(\gamma_f^*, \gamma_p^*)$  and  $(\gamma_f^o, \gamma_p^o)$  be defined as in Lemma 5.6. If  $\widetilde{K}$  tends to zero and  $m_{\max} > m_{\min}$ , then

(5.18) 
$$\rho(\gamma_f^*, \gamma_p^*, m_{\text{max}}) > \rho(\gamma_f^o, \gamma_p^o, m_c).$$

*Proof.* From the definition of  $m_c$  in (5.9), we find  $m_c \in \left[\frac{1}{\tilde{K}\gamma_f^o}, \frac{\gamma_f^o}{\tilde{K}(\gamma_f^*)^2}\right]$  and then obtain

$$\rho(\gamma_f^o, \gamma_p^o, m_c) = \frac{2\widetilde{\mu}}{\widetilde{K}} \left( \frac{-\widetilde{K}\gamma_f^* m_c + \frac{\gamma_f^o}{\gamma_f^*}}{2\widetilde{\mu} m_c \frac{\gamma_f^o}{\gamma_f^*} + \gamma_f^*} \right) \left( \frac{\widetilde{K}\gamma_f^o m_c - 1}{2\widetilde{\mu} m_c + \gamma_f^o} \right) = \frac{2\widetilde{\mu}}{\widetilde{K}} \frac{-a_2(m_c)}{b_2(m_c)},$$

where  $a_2(m_c)$  is negative and  $b_2(m_c)$  is positive. In order to ensure (5.18), we need only prove  $\frac{a_1(m_{\text{max}})}{b_1(m_{\text{max}})} > \frac{-a_2(m_c)}{b_2(m_c)}$  or  $\frac{a_1(m_{\text{max}})}{b_1(m_{\text{max}})} b_2(m_c) + \tilde{K}^2 m_c^2 \gamma_f^* \gamma_f^o + \frac{\gamma_f^o}{\gamma_f^*} > \tilde{K} m_c \left(\gamma_f^* + \frac{(\gamma_f^o)^2}{\gamma_f^*}\right)$ . Using Lemma 5.7, we obtain

$$\lim_{\widetilde{K}\to 0} \frac{\widetilde{K}^2 m_c^2 \gamma_f^* \gamma_f^o}{\widetilde{K} m_c \left(\gamma_f^* + \frac{\gamma_f^2}{\gamma_f^*}\right)} = \lim_{\widetilde{K}\to 0} \frac{\widetilde{K} m_c (\gamma_f^*)^2 \gamma_f^o}{(\gamma_f^*)^2 + (\gamma_f^o)^2} = \lim_{\widetilde{K}\to 0} m_c \frac{\left(\frac{1}{\bar{m}}\right)^2 \frac{2\bar{m}}{\bar{m}^2 + \hat{m}}}{\left(\frac{1}{\bar{m}}\right)^2 + \left(\frac{2\bar{m}}{\bar{m}^2 + \hat{m}}\right)^2}$$

$$= \lim_{\widetilde{K}\to 0} m_c \frac{2\bar{m} \left(\bar{m}^2 + \hat{m}\right)}{\left(\bar{m}^2 + \hat{m}\right)^2 + 4\bar{m}^4} = \frac{1}{2}.$$
(5.19)

Similarly, we have

$$\lim_{\tilde{K} \to 0} \frac{\frac{\gamma_f^c}{\gamma_f^*}}{\tilde{K} m_c \left(\gamma_f^* + \frac{(\gamma_f^c)^2}{\gamma_f^*}\right)} = 8 \left(\frac{\bar{m}^2 \left(\bar{m}^2 + \hat{m}\right)}{\left(\bar{m}^2 + \hat{m}\right)^2 + 4\bar{m}^4}\right)^2 := 8C_1,$$

(5.21)

$$\lim_{\widetilde{K}\to 0} \frac{a_1(m_{\max})}{b_1(m_{\max})} \frac{\gamma_f^* \gamma_f^o}{\widetilde{K} m_c \left(\gamma_f^* + \frac{(\gamma_f^o)^2}{\gamma_f^*}\right)} = 8 \left(\frac{2\bar{m}(m_{\max} - m_{\min}) \left(\bar{m}^2 + \widehat{m}\right)}{\left(\bar{m}^2 + \widehat{m}\right)^2 + 4\bar{m}^4}\right)^2 := 8C_2.$$

Let 
$$\zeta = \frac{m_{\text{max}}}{m_{\text{min}}}$$
 and  $f(\zeta) = C_1 + C_2 = \frac{2\zeta^8 + 28\zeta^7 + 128\zeta^6 + 228\zeta^5 + 252\zeta^4 + 228\zeta^3 + 128\zeta^2 + 28\zeta + 2}{(5\zeta^4 + 28\zeta^3 + 62\zeta^2 + 28\zeta + 5)^2}$ .  
From  $f'(\zeta) = \frac{-28\zeta^{10} + 2124\zeta^8 + 8448\zeta^7 + 9640\zeta^6 - 9640\zeta^4 - 8448\zeta^3 - 2124\zeta^2 + 28}{(5\zeta^4 + 28\zeta^3 + 62\zeta^2 + 28\zeta + 5)^3}$ , we find that  $f(\zeta)$ 

П

has only one local minimum  $\zeta_1 = 1$  and one local maximum  $\zeta_2 \approx 10.3942$  on interval  $[1, +\infty)$ . Further, from  $f(\zeta_1) = \frac{1}{16}$  and  $\lim_{\zeta \to +\infty} f(\zeta) = \frac{2}{25}$ , we know that  $f(\zeta) \ge \frac{1}{16}$  on interval  $[1, +\infty)$ . Using (5.19)–(5.21), when  $m_{\text{max}} > m_{\text{min}}$ , we obtain

$$\lim_{\widetilde{K} \to 0} \frac{a_1(m_{\text{max}})}{b_1(m_{\text{max}})} b_2(m_c) + \widetilde{K}^2 m_c^2 \gamma_f^* \gamma_f^o + \frac{\gamma_f^o}{\gamma_f^*} \\
> \lim_{\widetilde{K} \to 0} \left( \frac{1}{2} + \frac{8}{16} \right) \widetilde{K} m_c \left( \gamma_f^* + \frac{(\gamma_f^o)^2}{\gamma_f^*} \right) = \lim_{\widetilde{K} \to 0} \widetilde{K} m_c \left( \gamma_f^* + \frac{(\gamma_f^o)^2}{\gamma_f^*} \right),$$

which leads to (5.18).

Remark 5.9. Numerically, we observe that  $a_1(m_{\text{max}})b_2(m_c) + a_2(m_c)b_1(m_{\text{max}}) > 0$  for various choices of  $\widetilde{\mu}$  and  $\widetilde{K}$ , which means that the restriction on  $\widetilde{K}$  in Lemma 5.8 is not necessary for the inequality (5.18) in practice, but the corresponding analysis is still open for future work.

Theorem 5.10. Let  $(\gamma_f^*, \gamma_p^*)$  and  $(\gamma_f^*, \gamma_p^*)$  be the solution of (5.5) and Lemma 5.8, respectively. If  $\widetilde{K}$  tends to zero and  $m_{\max} > m_{\min}$ , then

(5.22) 
$$\max_{m \in [m_{\min}, m_{\max}]} \rho(\gamma_f^*, \gamma_p^*, m) > \max_{m \in [m_{\min}, m_{\max}]} \rho(\gamma_f^*, \gamma_p^*, m).$$

That is,

$$(5.23) \qquad \rho(\gamma_f^*, \gamma_p^*, m_{\min}) > \rho(\gamma_f^*, \gamma_p^*, m_{\min}), \ \rho(\gamma_f^*, \gamma_p^*, m_{\max}) > \rho(\gamma_f^*, \gamma_p^*, m_{\max}), \ \rho(\gamma_f^*, \gamma_p^*, m_{\max}) > \rho(\gamma_f^*, \gamma_p^*, m_c).$$

*Proof.* From the definition of  $(\gamma_f^o, \gamma_p^o)$ , we know that

$$\max_{m \in [m_{\min}, m_{\max}]} \rho(\gamma_f^o, \gamma_p^o, m) \geq \max_{m \in [m_{\min}, m_{\max}]} \rho(\gamma_f^\star, \gamma_p^\star, m).$$

Further, by Lemmas 5.6 and 5.8, we have

$$\max_{m \in [m_{\min}, m_{\max}]} \rho(\gamma_f^*, \gamma_p^*, m) > \max_{m \in [m_{\min}, m_{\max}]} \rho(\gamma_f^o, \gamma_p^o, m),$$

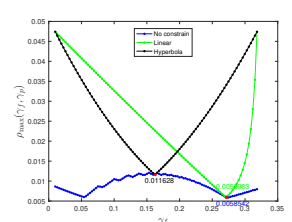
when  $\widetilde{K}$  tends to zero and  $m_{\text{max}} > m_{\text{min}}$ . From the fact  $\rho(\gamma_f^*, \gamma_p^*, m_{\text{min}}) = \rho(\gamma_f^*, \gamma_p^*, m_{\text{max}})$ , we finally obtain (5.22) and (5.23).

Remark 5.11. Here, in this work we discussed the hyperbolic and linear relations between  $\gamma_f$  and  $\gamma_p$ . It is also possible to design optimal parameters with no constraints between these parameters. In this case, we use the following procedure to numerically obtain the optimal pairs  $\{(\gamma_f^i, \gamma_p^{i, \diamond})\}_{i=0}^n$  and the corresponding maximum spectral radius:

- 1. Divide the interval  $\mathcal{I}_f$  into n equal subintervals and denote the node set by  $\left\{\gamma_f^i\right\}_{i=0}^n$ . Similarly, divide the interval  $\left[2\widetilde{\mu}m_{\min},2\widetilde{\mu}m_{\max}\right]$  into m equal subintervals and denote the node set by  $\left\{\gamma_p^j\right\}_{i=0}^m$ .
- 2. For each node  $\gamma_f^i$ , compute

$$\rho_{\max}^{i,j} = \max\left\{\rho(\gamma_f^i, \gamma_p^j, m_{\min}), \rho(\gamma_f^i, \gamma_p^j, m_{\max}), \rho(\gamma_f^i, \gamma_p^j, m_c)\right\}$$

for all  $\gamma_n^j$ .



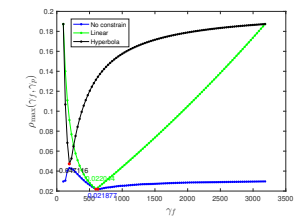


Fig. 8. Comparison of the maximum spectral radius with respect to  $\gamma_f$  for the min-max approach with  $m_{\min} = \pi, m_{\max} = \pi/h, h = 1/32$ , and  $\mu = 1, K = 1$  (left) or  $\mu = 1e - 1, K = 1e - 4$  (right).

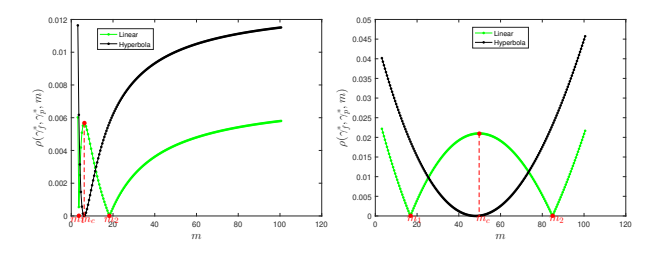


Fig. 9. Comparison of the spectral radius with respect to m for the min-max approach with  $m_{\min} = \pi, m_{\max} = \pi/h, h = 1/32, \text{ and } \mu = 1, K = 1 \text{ (left) or } \mu = 1e-1, K = 1e-4 \text{ (right)}.$ 

3. For each index i, find the index  $s_i \in \{0, \dots, m\}$  such that  $\rho_{\max}^{i, s_i}$  is the minimum of  $\{\rho_{\max}^{i, j}\}_{j=0}^m$  and then set  $\gamma_p^{i, \diamond} = \gamma_p^{i, s_i}$ .

However, the computational cost of this strategy is significantly increased because of the need to compute all the possible combinations of the discrete node sets of  $\gamma_f$  and  $\gamma_p$ . On the other hand, it produces absolute optimal parameters which are used to compare with the ones obtained with the hyperbolic and linear relations. In Figure 8, we compare the maximum spectral radius with respect to  $\gamma_f$  of the linear and hyperbolic relations with the nonconstraint technique, while in Figure 9 we show the spectral radius with respect to m under the optimal parameters of linear and hyperbolic relations. From these figures, we can make the following observations: (1) in Figure 8, the minimum point of the linear relation is smaller than that of the hyperbolic relation; (2) in Figure 8, the minimum point of the linear relation is closer to the one of the nonconstraint case than the one given by the hyperbolic relation; (3) in Figure 9, most of the spectral radii corresponding to the linear relation are smaller than those of the hyperbolic relation.

**5.2.2.** Minimization of the spectral expectation. Instead of the complex interval  $\mathcal{A}_f$ , we consider the simple interval  $\mathcal{I}_f$  and then minimize the expectation of  $\rho(\gamma_f, \gamma_p, m)$  in the interval  $[m_{\min}, m_{\max}]$ :

(5.24) 
$$\min_{\substack{\gamma_f \in \mathcal{I}_f \\ \gamma_p = p\gamma_f + q}} E(\gamma_f, \gamma_p),$$

where

$$E(\gamma_f, \gamma_p) := \frac{1}{m_{\text{max}} - m_{\text{min}}} \int_{m_{\text{min}}}^{m_{\text{max}}} \rho(\gamma_f, \gamma_p, m) dm$$

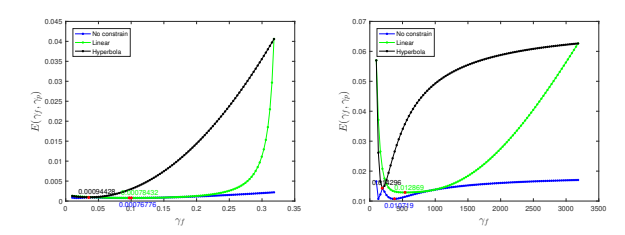


Fig. 10. Comparison of the maximum spectral radius with respect to  $\gamma_f$  for the expectation approach with  $m_{\min} = \pi, m_{\max} = \pi/h, h = 1/32$ , and  $\mu = 1, K = 1$  (left) or  $\mu = 1e - 1, K = 1e - 4$  (right).

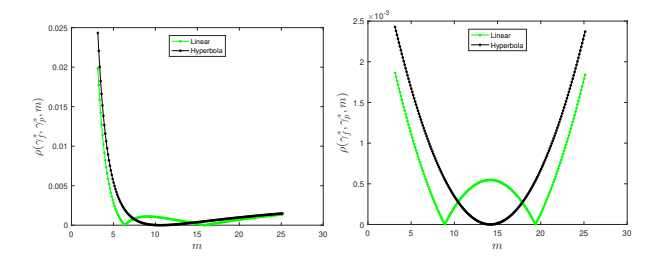


Fig. 11. Comparison of the spectral radius with respect to m for the expectation approach with  $m_{\min} = \pi, m_{\max} = \pi/h, h = 1/32, \text{ and } \mu = 1, K = 1 \text{ (left) or } \mu = 1e - 1, K = 1e - 4 \text{ (right)}.$ 

$$\begin{split} &= \frac{1}{m_{\max} - m_{\min}} \Bigg( \int_{m_{\min}}^{m_{1c}} -g(\gamma_f, \gamma_p, m) \mathrm{d}m + \int_{m_{1c}}^{m_{2c}} g(\gamma_f, \gamma_p, m) \mathrm{d}m \\ &+ \int_{m_{2c}}^{m_{\max}} -g(\gamma_f, \gamma_p, m) \mathrm{d}m \Bigg) \\ &= \frac{\left(\gamma_f + \gamma_p\right) \left(2\widetilde{\mu} + \widetilde{K}\gamma_p^2\right)}{\widetilde{K}\gamma_p^2 (m_{\max} - m_{\min}) \left(\gamma_f \gamma_p \widetilde{K} - 2\widetilde{\mu}\right)} \ln \left( \left(\frac{\widetilde{K}\gamma_p m_{\max} + 1}{\widetilde{K}\gamma_p m_{\min} + 1}\right) \left(\frac{\widetilde{K}\gamma_p m_{1c} + 1}{\widetilde{K}\gamma_p m_{2c} + 1}\right)^2 \right) \\ &- \frac{\left(\gamma_f + \gamma_p\right) \left(2\widetilde{\mu} + \widetilde{K}\gamma_f^2\right)}{2\widetilde{\mu} (m_{\max} - m_{\min}) \left(\gamma_f \gamma_p \widetilde{K} - 2\widetilde{\mu}\right)} \ln \left( \left(\frac{\gamma_f + 2\widetilde{\mu} m_{\max}}{\gamma_f + 2\widetilde{\mu} m_{\min}}\right) \left(\frac{\gamma_f + 2\widetilde{\mu} m_{1c}}{\gamma_f + 2\widetilde{\mu} m_{2c}}\right)^2 \right) \\ &+ \frac{\gamma_f}{\gamma_p} \left(1 - \frac{2(m_{2c} - m_{1c})}{m_{\max} - m_{\min}}\right). \end{split}$$

Since the expectation  $E(\gamma_f, \gamma_p)$  is continuous in the bounded interval  $[m_{\min}, m_{\max}]$ , there exists at least one minimum in  $[m_{\min}, m_{\max}]$ . Similar spectral distribution between the hyperbolic and linear relations is shown in Figures 10 and 11.

6. The Orthodir acceleration for the Robin–Robin algorithm. From the above analysis for the spectral radius of the Robin–Robin iterative operator, the convergence of the algorithm may not be guaranteed when using the successive approximation method because  $\rho(\mathcal{A}_m) < 1$  is not satisfied for any mode m ( $\rho(\mathcal{A}_0) = 1$ ). Therefore, in order to ensure this convergence, we use the Orthodir Krylov subspace method [58, 62] because of its simpler implementation. Denote Darcy equation (3.7)

and Stokes equations (3.6a)–(3.6b) by the algebraic systems

$$(6.1) A_1 u_1 = b_1 + l_1, A_2 u_2 = b_2 + l_2,$$

respectively. Here  $b_1$  and  $l_1$  correspond to the first and second terms of the right-hand side of (3.7), while  $b_2$  and  $l_2$  correspond to the first and second terms of the right-hand side of (3.6a) in addition to the right-hand side of (3.6b).

Now, set vectors  $X_1^k, X_2^k$  to be the algebraic forms corresponding to  $\eta_p^k, \eta_f^k$  on the interface  $\Gamma$ . Then, the updated vectors  $X_1^{k+1}, X_2^{k+1}$  can be obtained by the following processes:

- 1. Obtain the vectors  $b_1 = b_1(X_1^k), b_2 = b_2(X_2^k)$  for the algebraic systems (6.1) based on the vectors  $X_1^k, X_2^k$
- 2. Find the solutions  $u_1 = u_1(X_1^k), u_2 = u_2(X_2^k)$  of the algebraic systems and then extract the interface portions  $u_1^{\Gamma}$ ,  $u_2^{\Gamma}$  of the solutions  $u_1$ ,  $u_2$ , respectively. 3. Obtain the corresponding updated vectors  $X_1^{k+1}$ ,  $X_2^{k+1}$  according to the up-
- dated process (3.8).

Let  $X^k := (X_1^k, X_2^k)$  and  $\widehat{\mathcal{A}}X^k = X^{k+1}$ . Then the Robin-Robin decomposition algorithm can be treated as a Jacobi iteration of the problem

$$\widehat{\mathcal{A}}X = X.$$

Here, instead of the Jacobi iteration, we solve the problem (6.2) by the Orthodir algorithm. Set  $AX := \{\widehat{A}X | l_1 = 0, l_2 = 0\}$  and  $g_0 := \{\widehat{A}X | b_1 = 0, b_2 = 0\}$ . Then (6.2) can be rewritten as

(6.3) 
$$\widetilde{\mathcal{A}}X := (I - \mathcal{A})X = g_0,$$

where I is the identity operator. Then the Orthodir iterative processes of the problem (6.3) are as follows:

## Algorithm 6.1 Robin-Robin Orthodir DDM for Stokes-Darcy problem.

```
Set r^0 = p^0 = g_0.

for j = 0, 1, ... do
      Compute \mathcal{A}p^j by solving \widehat{\mathcal{A}}p^j with l_1=0 and l_2=0, and then set \widetilde{\mathcal{A}}p^j=p^j-\mathcal{A}p^j.
      Compute \mathcal{A}^2 p^j using the same routine but with \mathcal{A} p^j instead of p^j.
     \begin{split} \alpha_j &= \frac{\langle r^j, \widetilde{\mathcal{A}} p^j \rangle}{\langle \widetilde{\mathcal{A}} p^j, \widetilde{\mathcal{A}} p^j \rangle}. \\ X^{j+1} &= X^j + \alpha_j p^j. \end{split}
      r^{j+1} = r^j - \alpha_j \widetilde{\mathcal{A}} p^j.
      for i = 0, \ldots, j do
     \beta_{ij} = -\frac{\langle \widetilde{\mathcal{A}}^2 p^j, \widetilde{\mathcal{A}} p^j \rangle}{\langle \widetilde{\mathcal{A}} p^i, \widetilde{\mathcal{A}} p^i \rangle}.
end for
     p^{j+1} = \widetilde{\mathcal{A}}p^j + \sum_{i=0}^j \beta_{ij}p^i.
end for
```

Initialize  $X^0 = 0$ . Solve  $g_0 = \widehat{\mathcal{A}} X^0$ .

7. Numerical experiments. In this section, we provide some numerical experiments to verify the effectiveness of the newly derived optimal Robin parameters. The Taylor–Hood finite elements and the quadratic finite elements are considered to discretize the Stokes equations and the primary formulation of the Darcy equations, respectively. In the following tests, we set the mesh size h = 1/32 and the tolerance  $10^{-9}$  on relative residual as the stopping criterion for the Orthodir iterations.

All of the errors we compute in this section are the differences between the finite element solutions of the DDM and the corresponding coupled finite element solutions. Four different optimal approaches are considered in the following numerical experiments, including the min-max approach with linear relation (M-L), the min-max approach with hyperbolic relation (M-H), the expectation approaches with linear relation (E-L), and the expectation approaches with hyperbolic relation (E-H).

7.1. Geometry with straight interface. Consider the domain  $\Omega=(0,1)\times(0,2)$  where the Stokes region  $\Omega_S=(0,1)\times(1,2)$ , the Darcy region  $\Omega_D=(0,1)\times(0,1)$ , and the interface  $\Gamma=(0,1)\times\{1\}$ . Let  $\alpha=\alpha_0\sqrt{\frac{\mu}{K}}$  and  $\alpha_0=1,g=1,z=0$ . The boundary condition data functions and the source terms are set to satisfy the Stokes and Darcy equations by the following solution, respectively:

$$\phi_D = (-\alpha_0 x (y - 1) + y^3/3 - y^2 + y)/K + 2\mu x,$$
  
$$\mathbf{u}_S = (\sqrt{\mu K}, \alpha_0 x), \quad p_S = 2\mu (x + y - 1) + 1/(3K).$$

In Figures 12 and 13, we plot  $L^2$  errors in hydraulic head and Stokes velocity versus the number of iterations for two groups of parameters:  $\mu=1, K=1$  and  $\mu=1, K=10^{-2}$ . In Figure 12, we consider the nonoptimized Robin parameters from [9] which is for a Jacobi type solver. One can observe that Orthodir solver converges in the cases for which the Jacobi type solver diverges in [9]. Meanwhile, Orthodir solver also speeds up the convergence in the cases for which the Jacobi type method converges in [9]. In Figure 13, we consider the optimal Robin parameters obtained from the four different optimal approaches: M-L, M-H, E-L, and E-H. Then the number of iteration steps is significantly reduced, compared with the results in Figure 12.

Table 1 shows the values of the optimal Robin parameters and the corresponding numbers of iterations for different values of  $\mu$  and K and the four different optimal approaches, with  $m_{min} = \pi$  and  $m_{max} = \pi/h$ . Table 2 shows the errors for  $\mu = 1$  and  $K = 10^{-2}$  with various h and different optimal Robin parameters of four optimal approaches. One can observe that the optimal Robin parameters of four optimal approaches do not have much influence on the accuracy of the finite element solutions of the DDM.

Furthermore, when the domain decomposition iterations stop in Figures 12 and 13, the final errors are very small. Meanwhile, the final errors listed in Table 2 are also very small for various h (less than  $10^{-7}$ ). Recall that these final errors are the differences between the final finite element solutions of the DDM and the corresponding coupled finite element solutions. Since it is well known that the coupled finite element solutions for the Stokes–Darcy model have optimal accuracy orders in term of h [11, 19, 48], then it is easy to verify that the finite element solutions of the DDM also have optimal accuracy orders in term of h.

Finally, in Figure 14, we display the contour distributions of the number of iterations on the values of  $\gamma_f$  (x-coordinate) and  $\gamma_p$  (y-coordinate) for different settings of  $(\mu, K)$ , and mark the optimal Robin parameters.

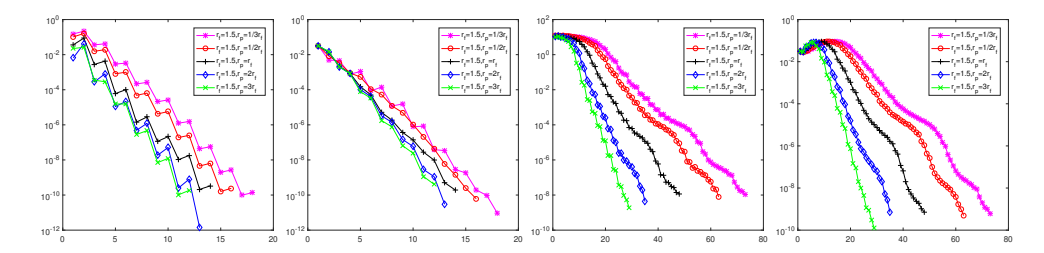


Fig. 12. Orthodir DDM results with nonoptimized Robin parameters:  $L^2$  hydraulic head errors  $e_\phi^k$  (the first and third plots) and  $L^2$  Stokes velocity errors  $e_u^k$  (the second and fourth plots), versus the number of iterations with h=1/32. Here  $\mu, K$  are set as  $\mu=1, K=1$  (the first two plots) and  $\mu=1, K=10^{-2}$  (the last two plots).

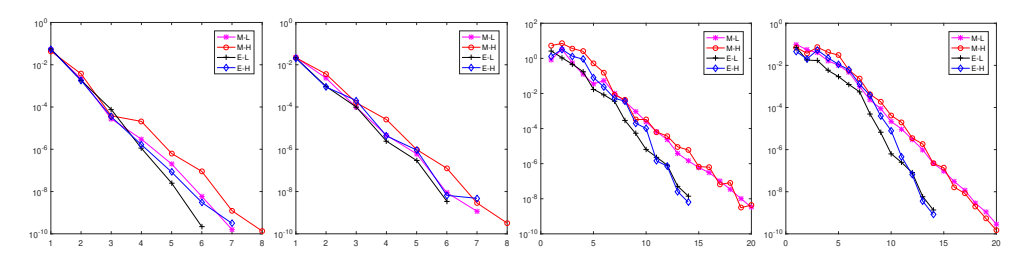


FIG. 13. Orthodir DDM results with optimal Robin parameters:  $L^2$  hydraulic head errors  $e_\phi^k$  (the first and third plots) and  $L^2$  Stokes velocity errors  $e_u^k$  (the second and fourth plots), versus the number of iterations with h=1/32. Here  $\mu,K$  are set as  $\mu=1,K=1$  (the first two plots) and  $\mu=1,K=10^{-2}$  (the last two plots).

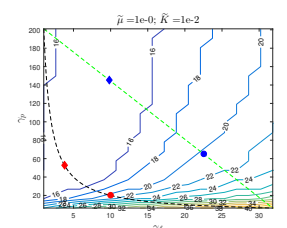
Table 1 The optimal parameter pairs  $(\gamma_f, \gamma_p)$  and the number of iterations for different  $\mu$  and K with four optimal approaches including M-L, M-H, E-L, and E-H.

$\mu$	K	$\gamma_f$	$\gamma_p$	$ ho_{ m max}$	$E(\gamma_f, \gamma_p)$	Iter	
1	1	0.2703	36.6256	0.0060	0.0041	7	(M-L)
		0.1618	12.3606	0.0116	0.0089	8	(M-H)
		0.1014	143.3135	0.0324	0.0008	6	(E-L)
		0.0363	55.1120	0.0393	0.0009	7	(E-H)
1	1e-6	5.6434e + 04	171.6983	0.0024	0.0014	18	(M-L)
		1.9245e + 04	103.9255	0.0048	0.0016	21	(M-H)
		5.6434e + 04	171.6983	0.0024	0.0014	18	(E-L)
		1.9245e + 04	103.9255	0.0048	0.0016	21	(E-H)
1e-1	1e-4	595.3315	16.9741	0.0222	0.0129	31	(M-L)
		207.9411	9.6181	0.0457	0.0145	33	(M-H)
		533.3490	17.3656	0.0260	0.0129	31	(E-L)
		192.4455	10.3926	0.0474	0.0143	33	(E-H)

Table 2

The errors for  $\mu=1$  and  $K=10^{-2}$  with different mesh sizes and different optimal Robin parameters of four optimal approaches including M-L, M-H, E-L, and E-H.

h	1/8	1/16	1/32	1/64	1/128	1/256	
	5.37e-09	2.54e-09	3.28e-09	2.18e-09	4.08e-09	2.24e-09	(M-L)
$L^2$ errors in hydraulic head	3.28e-09	2.13e-09	4.38e-09	2.61e-09	2.29e-09	2.08e-09	(M-H)
L- errors in hydraulic head	1.56e-09	3.62e-09	1.44e-08	5.11e-09	5.66e-08	8.10e-08	(E-L)
	7.02e-09	1.25 e-09	6.34 e-09	2.35e-09	4.81e-09	2.75e-08	(E-H)
	7.84e-10	3.78e-10	2.89e-10	3.00e-10	5.56e-10	4.61e-10	(M-L)
$L^2$ errors in Stokes velocity			1.47e-10				
L errors in Stokes velocity	3.52e-10	8.90e-10	1.38e-09	9.01e-10	1.23e-08	1.27e-08	(E-L)
	1.39e-10	$4.42\mathrm{e}\text{-}10$	8.19e-10	5.21e-10	8.20e-10	4.98e-09	(E-H)



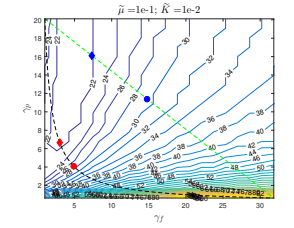


FIG. 14. Contour distribution of the number of iterations with  $(\mu, K) = (1, 1e - 2)$  (left) and  $(\mu, K) = (1e - 1, 1e - 2)$  (right). Here four optimal parameter pairs  $(\gamma_f, \gamma_p)$  are marked by blue circle (M-L), blue diamond (E-L), red circle (M-H), and red diamond (E-L), respectively. (Figure in color online.)

Table 3 The optimal parameter pairs  $(\gamma_f, \gamma_p)$  and the numbers of iterations for different  $\mu$ , K, and h with four optimal approaches including M-L, M-H, E-L, and E-H.

$(\mu, K)$	h = 1/8			h = 1/32			h = 1/128			
	$\gamma_f$	$\gamma_p$	${\rm Iter}$	$\gamma_f$	$\gamma_p$	Iter	$\gamma_f$	$\gamma_p$	${\rm Iter}$	
(1,1)	2.44e-01	1.80e + 01	12	2.70e-01	3.66e + 01	10	2.66e-01	1.39e + 02	10	(M-L)
	1.77e-01	1.13e+01	12	1.62e-01	1.24e+01	10	1.58e-01	1.27e + 01	10	(M-H)
	1.57e-01	3.17e + 01	12	1.01e-01	1.43e+02	10	5.01e-02	6.84e + 02	10	(E-L)
	9.44e-02	2.12e+01	12	3.63e-02	$5.51e{+01}$	10	1.20e-02	1.67e + 02	10	(E-H)
	1.91e+01	2.64e+01	24	2.25e+01	6.50e + 01	24	2.28e+01	2.35e+02	24	(M-L)
(1.15.9)	1.22e+01	1.63e + 01	25	9.98e + 00	2.00e+01	22	9.29e+00	2.15e+01	22	(M-H)
(1,1e-2)	1.42e+01	3.41e + 01	22	9.83e+00	1.45e + 02	24	5.96e+00	6.60e + 02	24	(E-L)
	8.74e + 00	$2.29e{+01}$	23	3.78e + 00	$5.29e{+01}$	26	1.52e+00	1.32e+02	30	(E-H)
	1.15e+01	3.83e-01	35	7.89e + 00	1.57e + 00	37	8.34e+00	6.00e+00	35	(M-L)
(1. 9.1. 9)	7.20e+00	2.78e-01	35	2.54e+00	7.86e-01	37	1.68e + 00	1.19e+00	31	(M-H)
(1e-2,1e-2)	1.14e+01	3.86e-01	35	5.33e+00	1.74e + 00	33	2.31e+00	7.52e + 00	40	(E-L)
	7.20e+00	2.78e-01	35	2.23e+00	8.95 e-01	33	8.84e-01	2.26e+00	38	(E-H)
(1e-6,1e-6)	1.13e+05	3.88e-05	9	5.64e + 04	1.72e-04	9	5.49e + 04	6.72e-04	11	(M-L)
	7.06e + 04	2.83e-05	9	1.92e+04	1.04e-04	9	5.66e + 03	3.53e-04	11	(M-H)
	1.13e+05	3.88e-05	9	5.80e + 04	1.71e-04	9	8.66e + 04	5.92e-04	11	(E-L)
	7.06e + 04	2.83e-05	9	1.92e+04	1.04e-04	9	5.66e + 03	3.53e-04	11	(E-H)

7.2. Geometry with curved interface. Consider the domain  $\Omega = (-1.5, 1.5) \times (-1.5, 1.5)$  and set the interface  $\Gamma$  as  $y = -0.5\sin(\pi(x+1.5)), -1.5 \le x \le 1.5$ . The Stokes and Darcy regions are the top and bottom parts of  $\Omega$  sharing the interface  $\Gamma$ , respectively. On the Stokes boundary excluding the interface, we impose  $\mathbf{u}_S = (0, x^2 - 4)$  as a boundary condition. For the Darcy boundary excluding the interface, we impose impermeability boundary condition  $\mathbb{K}\nabla\phi_D\cdot\mathbf{n}_D=0$  on the left and the right boundary and homogeneous Dirichlet boundary condition on the bottom boundary. The source terms of the Stokes and Darcy equations are given by  $\mathbf{f}_S = 0, f_D = 0$ . In the following tests, we set  $\alpha = \sqrt{\frac{\mu}{K}}, g = 1, z = 0$ . Table 3 reports the optimal Robin parameters and the number of iterations for different  $\mu$ , K, and h with the four optimal approaches. When h decreases, the numbers of iterations do not grow much for all the four optimal approaches and all pairs of  $\mu$  and K used in the test. Figure 15 shows the numerical solutions for  $\mu = 1$  and  $K = 10^{-2}$ .

These numerical experiments show the effectiveness of the new Orthodir DDM algorithm where the optimized parameters are computed using the linear relation. In particular, it shows that this new linear relation is another robust strategy in the optimization process of these Robin parameters. Figure 13, Table 1, and Table 3 show comparable results with the ones obtained using the hyperbolic relation [17].

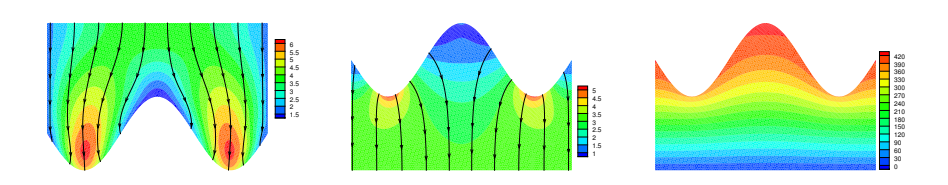


FIG. 15. Stokes velocity magnitude and streamline (left), Darcy velocity magnitude and streamline (middle), and Darcy pressure (right) with  $(\mu, K) = (1, 10^{-2})$  (right).

8. Conclusions. In this paper we proposed a new strategy in the optimization of domain decomposition algorithms based on Robin type boundary conditions for the Stokes-Darcy system. We performed a modal analysis on a geometry with circular interfaces and introduced a new linear relation connecting the Robin parameters. Using this relation with the min-max and the expectation minimization approaches, we derived optimal parameters that generate an improved distribution of eigenvalues of the iteration operator. This accelerates the convergence of the iterative procedure using Krylov subspaces methods. The numerical results confirm the effectiveness of the presented optimal parameters for geometries with straight and curved interfaces.

## REFERENCES

- [1] T. Arbogast and D. S. Brunson, A computational method for approximating a Darcy-Stokes system governing a vuggy porous medium, Comput. Geosci., 11 (2007), pp. 207–218.
- T. Arbogast and M. Gomez, A discretization and multigrid solver for a Darcy-Stokes system of three dimensional vuggy porous media, Comput. Geosci., 13 (2009), pp. 331–348.
- [3] L. Badea, M. Discacciati, and A. Quarteroni, Numerical analysis of the Navier-Stokes/Darcy coupling, Numer. Math., 115 (2010), pp. 195-227.
- [4] D. Bennequin, M. J. Gander, L. Gouarin, and L. Halpern, Optimized Schwarz waveform relaxation for advection reaction diffusion equations in two dimensions, Numer. Math., 134 (2016), pp. 513–567.
- [5] Y. BOUBENDIR, An analysis of the BEM-FEM non-overlapping domain decomposition method for a scattering problem, J. Comput. Appl. Math., 204 (2007), pp. 282–291.
- [6] Y. BOUBENDIR AND S. TLUPOVA, Stokes-Darcy boundary integral solutions using preconditioners, J. Comput. Phys., 228 (2009), pp. 8627–8641.
- Y. BOUBENDIR AND S. TLUPOVA, Domain decomposition methods for solving Stokes-Darcy problems with boundary integrals, SIAM J. Sci. Comput., 35 (2013), pp. B82–B106, https://doi.org/10.1137/110838376.
- [8] J. CAMANO, G. N. GATICA, R. OYARZUA, R. RUIZ-BAIER, AND P. VENEGAS, New fully-mixed finite element methods for the Stokes-Darcy coupling, Comput. Methods Appl. Mech. Engrg., 295 (2015), pp. 362–395.
- Y. CAO, M. GUNZBURGER, X.-M. HE, AND X. WANG, Robin-Robin domain decomposition methods for the steady Stokes-Darcy model with Beaver-Joseph interface condition, Numer. Math., 117 (2011), pp. 601–629.
- [10] Y. CAO, M. GUNZBURGER, X.-M. HE, AND X. WANG, Parallel, non-iterative, multi-physics domain decomposition methods for time-dependent Stokes-Darcy systems, Math. Comp., 83 (2014), pp. 1617–1644.
- [11] Y. CAO, M. GUNZBURGER, X. HU, F. HUA, X. WANG, AND W. ZHAO, Finite element approximation for Stokes-Darcy flow with Beavers-Joseph interface conditions, SIAM. J. Numer. Anal., 47 (2010), pp. 4239–4256, https://doi.org/10.1137/080731542.
- [12] Y. CAO, M. GUNZBURGER, F. HUA, AND X. WANG, Coupled Stokes-Darcy model with Beavers-Joseph interface boundary condition, Commun. Math. Sci., 8 (2010), pp. 1–25.
- [13] A. ÇEŞMELIOĞLU AND B. RIVIÈRE, Primal discontinuous Galerkin methods for time-dependent

- coupled surface and subsurface flow, J. Sci. Comput., 40 (2009), pp. 115-140.
- [14] W. CHEN, M. GUNZBURGER, F. HUA, AND X. WANG, A parallel Robin-Robin domain decomposition method for the Stokes-Darcy system, SIAM. J. Numer. Anal., 49 (2011), pp. 1064–1084, https://doi.org/10.1137/080740556.
- [15] P. CHIDYAGWAI AND B. RIVIÈRE, On the solution of the coupled Navier-Stokes and Darcy equations, Comput. Methods Appl. Mech. Engrg., 198 (2009), pp. 3806–3820.
- [16] M. DISCACCIATI, Domain Decomposition Methods for the Coupling of Surface and Groundwater Flows, Ph.D. thesis, Ecole Polytechnique Fédérale de Lausanne, Switzerland, 2004.
- [17] M. DISCACCIATI AND L. GERARDO-GIORDA, Optimized Schwarz methods for the Stokes-Darcy coupling, IMA J. Numer. Anal., 38 (2018), p. 1959–1983.
- [18] M. DISCACCIATI, P. GERVASIO, A. GIACOMINI, AND A. QUARTERONI, The interface control domain decomposition method for Stokes-Darcy coupling, SIAM J. Numer. Anal., 54 (2016), pp. 1039–1068, https://doi.org/10.1137/15M101854X.
- [19] M. DISCACCIATI, E. MIGLIO, AND A. QUARTERONI, Mathematical and numerical models for coupling surface and groundwater flows, Appl. Numer. Math., 43 (2002), pp. 57–74.
- [20] M. DISCACCIATI AND R. OYARZÚA, A conforming mixed finite element method for the Navier-Stokes/Darcy coupled problem, Numer. Math., 135 (2017), pp. 571–606.
- [21] M. DISCACCIATI AND A. QUARTERONI, Convergence analysis of a subdomain iterative method for the finite element approximation of the coupling of Stokes and Darcy equations, Comput. Vis. Sci., 6 (2004), pp. 93–103.
- [22] M. DISCACCIATI, A. QUARTERONI, AND A. VALLI, Robin-Robin domain decomposition methods for the Stokes-Darcy coupling, SIAM J. Numer. Anal., 45 (2007), pp. 1246–1268, https://doi.org/10.1137/06065091X.
- [23] O. Dubois, M. J. Gander, S. Loisel, A. St-Cyr, and D. B. Szyld, The optimized Schwarz method with a coarse grid correction, SIAM J. Sci. Comput., 34 (2012), pp. A421–A458, https://doi.org/10.1137/090774434.
- [24] V. J. ERVIN, E. W. JENKINS, AND S. SUN, Coupled generalized nonlinear Stokes flow with flow through a porous medium, SIAM J. Numer. Anal., 47 (2009), pp. 929–952, https: //doi.org/10.1137/070708354.
- [25] M. J. Gander, Optimized Schwarz methods, SIAM J. Numer. Anal., 44 (2006), pp. 699-731, https://doi.org/10.1137/S0036142903425409.
- [26] M. J. GANDER AND F. KWOK, Best Robin parameters for optimized Schwarz methods at cross points, SIAM J. Sci. Comput., 34 (2012), pp. A1849–A1879, https://doi.org/10.1137/ 110837218.
- [27] M. J. GANDER, F. MAGOULÈS, AND F. NATAF, Optimized Schwarz methods without overlap for the Helmholtz equation, SIAM J. Sci. Comput., 24 (2002), pp. 38–60, https://doi.org/10. 1137/S1064827501387012.
- [28] M. J. GANDER AND T. VANZAN, Heterogeneous optimized Schwarz methods for second order elliptic PDEs, SIAM J. Sci. Comput., 41 (2019), pp. A2329–A2354, https://doi.org/10. 1137/18M122114X.
- [29] M. J. GANDER AND Y. Xu, Optimized Schwarz methods with nonoverlapping circular domain decomposition, Math. Comp., 86 (2017), pp. 637-660.
- [30] M. J. GANDER AND H. ZHANG, A class of iterative solvers for the Helmholtz equation: Factorizations, sweeping preconditioners, source transfer, single layer potentials, polarized traces, and optimized Schwarz methods, SIAM Rev., 61 (2019), pp. 3–76, https://doi.org/10.1137/16M109781X.
- [31] Y. GAO, D. HAN, X.-M. HE, AND U. RÜDE, Unconditionally stable numerical methods for Cahn-Hilliard-Navier-Stokes-Darcy system with different densities and viscosities, J. Comput. Phys., 454 (2022), 110968.
- [32] Y. GAO, X.-M. HE, L. MEI, AND X. YANG, Decoupled, linear, and energy stable finite element method for the Cahn-Hilliard-Navier-Stokes-Darcy phase field model, SIAM J. Sci. Comput., 40 (2018), pp. B110-B137, https://doi.org/10.1137/16M1100885.
- [33] G. N. GATICA, S. MEDDAHI, AND R. OYARZÚA, A conforming mixed finite-element method for the coupling of fluid flow with porous media flow, IMA J. Numer. Anal., 29 (2009), pp. 86–108.
- [34] G. GIGANTE, M. POZZOLI, AND C. VERGARA, Optimized Schwarz methods for the diffusion-reaction problem with cylindrical interfaces, SIAM J. Numer. Anal., 51 (2013), pp. 3402–3430, https://doi.org/10.1137/120887758.
- [35] G. GIGANTE, G. SAMBATARO, AND C. VERGARA, Optimized Schwarz methods for spherical interfaces with application to fluid-structure interaction, SIAM J. Sci. Comput., 42 (2020), pp. A751–A770, https://doi.org/10.1137/19M1272184.
- [36] V. GIRAULT AND B. RIVIÈRE, DG approximation of coupled Navier-Stokes and Darcy equa-

- tions by Beaver–Joseph–Saffman interface condition, SIAM J. Numer. Anal., 47 (2009), pp. 2052–2089, https://doi.org/10.1137/070686081.
- [37] M. GUNZBURGER, X.-M. HE, AND B. LI, On Stokes-Ritz projection and multistep backward differentiation schemes in decoupling the Stokes-Darcy model, SIAM J. Numer. Anal., 56 (2018), pp. 397-427, https://doi.org/10.1137/16M1099601.
- [38] X.-M. HE, N. JIANG, AND C. QIU, An artificial compressibility ensemble algorithm for a stochastic Stokes-Darcy model with random hydraulic conductivity and interface conditions, Internat. J. Numer. Methods Engrg., 121 (2020), pp. 712-739.
- [39] X.-M. HE, J. LI, Y. LIN, AND J. MING, A domain decomposition method for the steadystate Navier-Stokes-Darcy model with Beavers-Joseph interface condition, SIAM J. Sci. Comput., 37 (2015), pp. S264-S290, https://doi.org/10.1137/140965776.
- [40] R. HOPPE, P. PORTA, AND Y. VASSILEVSKI, Computational issues related to iterative coupling of subsurface and channel flows, Calcolo, 44 (2007), pp. 1–20.
- [41] J. Hou, D. Hu, X.-M. He, and C. Qiu, Modeling and a Robin-type decoupled finite element method for dual-porosity-Navier-Stokes system with application to flows around multistage fractured horizontal wellbore, Comput. Methods Appl. Mech. Engrg., 388 (2022), 114248.
- [42] J. HOU, M. QIU, X.-M. HE, C. GUO, M. WEI, AND B. BAI, A dual-porosity-Stokes model and finite element method for coupling dual-porosity flow and free flow, SIAM J. Sci. Comput., 38 (2016), pp. B710–B739, https://doi.org/10.1137/15M1044072.
- [43] I. IGREJA AND A. F. D. LOULA, A stabilized hybrid mixed DGFEM naturally coupling Stokes-Darcy flows, Comput. Methods Appl. Mech. Engrg., 339 (2018), pp. 739-768.
- [44] C. Japhet and F. Nataf, The best interface conditions for domain decomposition methods: Absorbing boundary conditions, in Absorbing Boundaries and Layers, Domain Decomposition Methods, Nova Sci. Publ., Huntington, NY, 2001, pp. 348–373.
- [45] I. Jones, Low Reynolds number flow past a porous spherical shell, Proc. Cambridge Philos. Soc., 73 (1973), pp. 231–238.
- [46] G. Kanschat and B. Riviére, A strongly conservative finite element method for the coupling of Stokes and Darcy flow, J. Comput. Phys., 229 (2010), pp. 5933–5943.
- [47] W. LAYTON, H. TRAN, AND C. TRENCHEA, Analysis of long time stability and errors of two partitioned methods for uncoupling evolutionary groundwater-surface water flows, SIAM J. Numer. Anal., 51 (2013), pp. 248–272, https://doi.org/10.1137/110834494.
- [48] W. J. LAYTON, F. SCHIEWECK, AND I. YOTOV, Coupling fluid flow with porous media flow, SIAM J. Numer. Anal., 40 (2002), pp. 2195–2218, https://doi.org/10.1137/ S0036142901392766.
- [49] R. Li, J. Li, X.-M. He, and Z. Chen, A stabilized finite volume element method for a coupled Stokes-Darcy problem, Appl. Numer. Math., 133 (2018), pp. 2–24.
- [50] P.-L. LIONS, On the Schwarz alternating method. III. A variant for nonoverlapping subdomains, in Third International Symposium on Domain Decomposition Methods for Partial Differential Equations (Houston, TX, 1989), SIAM, Philadelphia, 1990, pp. 202–223.
- [51] K. LIPNIKOV, D. VASSILEV, AND I. YOTOV, Discontinuous Galerkin and mimetic finite difference methods for coupled Stokes-Darcy flows on polygonal and polyhedral grids, Numer. Math., 126 (2014), pp. 321–360.
- [52] Y. LIU, Y. HE, X. LI, AND X.-M. HE, A novel convergence analysis of Robin-Robin domain decomposition method for Stokes-Darcy system with Beavers-Joseph interface condition, Appl. Math. Lett., 119 (2021), 107181.
- [53] S. LOISEL AND D. B. SZYLD, On the geometric convergence of optimized Schwarz methods with applications to elliptic problems, Numer. Math., 114 (2010), pp. 697–728.
- [54] M. A. A. Mahbub, X.-M. He, N. J. Nasu, C. Qiu, and H. Zheng, Coupled and decoupled stabilized mixed finite element methods for nonstationary dual-porosity-Stokes fluid flow model, Internat. J. Numer. Methods Engrg., 120 (2019), pp. 803–833.
- [55] M. Mu And J. Xu, A two-grid method of a mixed Stokes-Darcy model for coupling fluid flow with porous media flow, SIAM J. Numer. Anal., 45 (2007), pp. 1801–1813, https: //doi.org/10.1137/050637820.
- [56] M. Mu And X. Zhu, Decoupled schemes for a non-stationary mixed Stokes-Darcy model, Math. Comp., 79 (2010), pp. 707–731.
- [57] B. RIVIÈRE AND I. YOTOV, Locally conservative coupling of Stokes and Darcy flows, SIAM J. Numer. Anal., 42 (2005), pp. 1959–1977, https://doi.org/10.1137/S0036142903427640.
- [58] Y. SAAD, Iterative Methods for Sparse Linear Systems, 2nd ed., SIAM, Philadelphia, PA, 2003, https://doi.org/10.1137/1.9780898718003.
- [59] P. SAFFMAN, On the boundary condition at the interface of a porous medium, Stud. in Appl. Math., 1 (1971), pp. 77–84.
- [60] D. VASSILEV, C. WANG, AND I. YOTOV, Domain decomposition for coupled Stokes and Darcy

- $\mathit{flows},$  Comput. Methods Appl. Mech. Engrg., 268 (2014), pp. 264–283.
- [61] Z. Yang, J. Ming, X.-M. He, and M. Li, A multigrid multilevel Monte Carlo method for Stokes-Darcy model with random hydraulic conductivity and Beavers-Joseph condition, J. Sci. Comput., 90 (2022), 68.
- [62] D. M. YOUNG AND K. C. Jea, Generalized conjugate-gradient acceleration of nonsymmetrizable iterative methods, Linear Algebra Appl., 34 (1980), pp. 159–194.